New Single Particle Methods for Detection and Characterization of Nanoparticles in Environmental Samples

Jani Tuoriniemi
Institutionen för kemi och molekylärbiologi
Naturvetenskapliga fakulteten

Akademisk avhandling för filosofie doktorsexamen i naturvetenskap, inriktning kemi som med tillstånd från Naturvetenskapliga fakulteten kommer att offentligt försvaras tisdagen den 1a okt, 2013 kl. 13:15 i sal KA, Institutionen för kemi och molekylärbiologi, Kemigården 4, Göteborg.

ISBN: 978-91-628-8769-8

New Single Particle Methods for Detection and Characterization of Nanoparticles in Environmental Samples

Department of chemistry and molecular biology
University of Gothenburg
SE-412 96 Gothenburg Sweden

ISBN: 978-91-628-8769-8

Life is so short, and the craft takes so long to learn

Geoffrey Chaucer

ABSTRACT

Nanoparticles (NP) are being used in rapidly increasing quantities which has resulted in concerns about possible harmful effects for health and environment. NP are already undergoing similar risk assessment programs as conventional chemicals, and due to their enhanced surface reactivities it has been proposed that the use of NP should be regulated by specific legislation based on particle size.

Number based concentrations and size distributions are thought to be more relevant dose metrics for toxicology than the mass of NP. Because NP are prone to processes such as aggregation, dissolution, or adsorption on surfaces characterization is required during the whole test. To measure the emission of NP and exposure levels in the environment the methods have to be capable of quantifying and sizing particles of interest at parts per billion level concentrations or lower.

Nanoparticle tracking analysis (NTA) was evaluated for measurement of number concentration and size distributions. The technique was considered suitable for monitoring and measuring exposure at relatively high ($> 10^6$ particles mL^{-1}) concentrations; however, NTA is relatively unspecific in the sense that it is difficult to distinguish particles of different materials.

To increase sensitivity and specificity single particle inductively coupled plasma mass spectrometry (spICP-MS) was developed for element specific characterization of particles in liquid samples. Validation of both the number concentration and sizing capabilities was carried out at concentrations as low as 10^2 particles mL^{-1}.The capabilities of spICP-MS as a fast screening tool for NP was evaluated, and the method was used to quantify trace level contamination of WC particles emitted from wear of winter tire studs and hard coatings.

Variable pressure or environmental scanning electron microscopes (ESEM) can be applied on a waist range of sample types with no or very little sample preparation. Therefore backscattered electron (BSE) imaging in such instrument was chosen as a base for developing a method for quantification of particles in solid samples. The technique was applied for quantifying particles in toxicity tests involving soil biota, and was concluded to be sensitive enough to cover the concentration range that is typically of interest in such tests.

Finally it was concluded that due to the tremendous amount of information obtained on a single particle basis, electron microscopy is a suitable complementing technique for spICP-MS measurements, which otherwise give little information about the structure of the particles.

Keywords: Nanoparticle Metrology Trace particle Characterisation Number concentration

 ISBN: 978-91-628-8769-8

POPULÄRVETENSKAPLIG SAMMANFATTNING PÅ SVENSKA

Nanopartiklar (NP) är partiklar som är mellan 1-100 nanometer stora. De har i vissa hänseenden egenskaper som påminner om lösta ämnen, i vissa fall mer som fasta substanser och ibland beter de sig på ganska oförutsägbara sätt med avseende på deras rörlighet och kemiska reaktivitet. NP i miljön är ett alltmer uppmärksammat problemområde. Även om det finns naturliga NP så sker det utsläpp av oavsiktligt producerade NP från t.ex. trafik, förbränning, och industriella processer. Men därutöver ökar användningen av syntetiskt tillverkade nanomaterial i samhället bland annat som ett resultat av implementeringen av nanoteknik i allt fler konsumentprodukter. Det råder en ökad oro i samhället och ett intresse från forskning och reglerande myndigheter att undersöka vilka möjliga risker för människor och ekosystem som kan föreligga med utsläpp av dessa syntetiska nanopartiklar. Inledande forskning har visat att det inte räcker att uppskatta riskerna med nanomaterial genom att relatera till dess samlade massa, då den specifika ytan är enormt mycket större än den hos makroskopiska fasta material. De reaktiva egenskaperna hos NP är oftast knutet just till ytan. Det har därför lyfts fram i ett antal inflytelserika forsknings och regulatoriska rapporter att partikelstorlek och antalskoncentrationen av de syntetiska partiklarna måste mätas för att kunna följa trender i miljön och förstå i vilken omfattning speciell risk föreligger. Tillämpbara metoder har dock saknats, och föremålet för detta avhandlingsarbete har därför varit att utforska och utveckla analysmetoder som kan stödja riskforskningen kring nanomaterial och nanopartiklar.

Huvudsakligen har tre analystekniker utvecklats under avhandlingsarbetet, för tre olika syften. Den första heter Nanoparticle Tracking Analysis (NTA) och var ett nytt instrument som verkade lovande för att mäta partikelantal och storleksfördelning av nanopartiklar. Metoden har utforskats, och trots att resultaten är i viss mån beroende av subjektivt bestämda parametrar, och att den uppmätta fördelningen av storlekar i vissa fall har en överrepresentation av stora partiklar, har NTA redan blivit en relativt etablerad teknik för analys och karaktärisering av NP i ekotoxikologiska studier. Detta är mycket på grund av det enkla handhavandet, höga känsligheten, samt att eventuella riktigt stora partiklar sällan interfererar med mätningarna. Däremot saknar NTA möjlighet att särskilja nanopartiklar av olika sammansättning från varandra, vilket är nödvändigt när man analyserar komplexa miljöprover med mycket bakgrundspartiklar. För det syftet har single particle ICP-MS utvecklats.

Single particle ICP-MS tekniken kan förenklat beskrivas som en partikelräknare som både räknar och bestämmer storleken på partiklarna i inflödet till instrumentet. Detta sker under förutsättning att dessa är rika på det grundämne som instrumentet är satt att övervaka. Metoden konstaterades vara mycket användbar då den kunde mäta partiklar i de låga koncentrationer som förekom i proven samt noggrannheten i antals och storleksbestämning var tillräkligt hög.

Fasta prov som jord och sediment är viktiga då det finns forskning som tyder på att nanopartiklar anrikas där, samt på grund av att det finns standardiserade ekotoxikologiska tester som involverar jordlevande organismer. Svepelektron mikroskopi användes för att kvantifiera partiklar i dessa prov.

Slutligen användes de nyligen nämnda, samt några ytterligare tekniker i kombination för att kvantifiera och karakterisera volframkarbid partiklar som emitteras på grund av slitage på dubbdäck och hårdmetall beläggningar.

PART A TABLE OF CONTENTS

PART B: SCIENTIFIC PAPERS INCLUDED

I. Gallego-Urrea, J. A., Tuoriniemi, J., Pallander, T. and Hassellöv, M. Measurements of nanoparticle number concentrations and size distributions in contrasting aquatic environments using nanoparticle tracking analysis. *Environmental Chemistry*. **2010**;7(1):67-81.

II. Gallego-Urrea, J. A., Tuoriniemi, J. and Hassellöv, M. Applications of particle-tracking analysis to the determination of size distributions and concentrations of nanoparticles in environmental, biological and food samples. *Trac-Trends in Analytical Chemistry*. **2011**;30(3):473-83.

III. Tuoriniemi, J., Johnsson, A.-C. J .H., Holmberg J. P., Gustafsson, S., Gallego-Urrea, J. A., Olsson, E., Pettersson, J. B. C. and Hassellöv, M.. Intermethod Comparison of the Particle Size Distributions of Colloidal Silica Nanoparticles. Submitted to *Particles and Particle Systems Characterization*

IV. Tuoriniemi, J., Gustafsson, S., Olsson, E. and Hassellöv, M. In situ characterization of physicochemical state and concentration of nanoparticles in soil ecotoxicity studies using an Environmental Scanning Electron Microscopy method. Submitted to *Environmental Chemistry*

V. Tuoriniemi, J., Cornelis, G. and Hassellöv, M. Improving Accuracy of Single particle ICPMS for Measurement of Size Distributions and Number Concentrations of Nanoparticles by Determining Analyte Partitioning During Nebulisation. Submitted to *Journal of Analytical Atomic Spectroscopy*

VI. Tuoriniemi J, Cornelis G, Hassellöv M. Size Discrimination and Detection Capabilities of Single-Particle ICPMS for Environmental Analysis of Silver Nanoparticles. *Analytical Chemistry*. **2012**;84(9):3965-72.

VII. Farkas J., Peter H., Christian P., Gallego-Urrea J. A., Hassellöv, M., Tuoriniemi, J., Gustafsson, S., Olsson, E., Hylland, K. and Thomas, K. V. Characterization of the effluent from a nanosilver producing washing machine. *Environment International*. **2011**;37(6):1057-62.

VIII. Hassellöv, M. Tuoriniemi, J., Gustafsson, S., Baumann, K. and Stolpe, B. Detection of manufactured nanomaterials in the environment. *Manuscript*

Contribution Report

There are multiple authors on the papers presented here and my contribution to each of them is listed below.

Paper I Had a significant contribution in performing the experiments analysing the data, and writing the paper

Paper II Developed the model for the dependence of NTA sensitivity on the particles ability to scatter light. Minor contribution for writing the other parts of the article.

Paper III Performed sedFFF experiments and assisted in electron microscopy and ES-SMPS measurements. Major part of writing and interpretation of the results.

Paper IV major part of planning, performing, and interpreting the outcome of the experiments and writing the paper.

Paper V major part of planning, performing, and interpreting the outcome of the experiments and writing the paper.

Paper VI significant contributions for planning and writing. Major part of performing the experiments and interpreting the the data.

Paper VII Performed and interpreted the single particle masspectrometry measurements

Paper VIII Performed and interpreted results of SEM and standalone spICPMS. Significant contribution to the TEM measurements.

List of abbreviations

NP	Nanoparticles
MNP	Manufactured nanoparticles
ENP	Engineered nanoparticles
PSD	Particle size distribution
TEM	Transmission electron microscopy
SEM	Scanning electron microscopy
DLS	Dynamic light scattering
ESD	equivalent spherical diameters
ICPMS	inductively coupled plasma mass spectrometry
spICP-MS	Single particle ICPMS
FFF	Field-Flow Fractionation
NTA	Nanoparticle Tracking Analsysis
ES-SMPS	Electrospray scanning mobility particle sizer
EDX	Energy dispersive X-ray Spectroscopy
SAED	Selected area electron microscopy
SE	Secondary electron imaging
BSE	Back scattered electron imaging
ROS	Reactive oxygen species
WWTP	Waste water treatment plant
NOM	Natural organic matter
MDMI	Monodisperse dried microparticle injector
CRM	Certified reference material
WC	Tungsten carbide
WC-Co	Cobalt cemented tungsten carbide

1. INTRODUCTION

1.1. NANOMATERIALS IN THE ENVIRONMENT

Although natural nanoparticles (NP) and nanomaterials (NM) have always been ubiquitous in the environment, both as incidental and manufactured anthropogenic NM with different compositions, shapes and reactivities are becoming increasingly abundant. Incidental NP can be released as a result of exhaust from cars, airplane and shipping, friction wear, electric motors, demolition, and industrial processes. Engineered or manufactured NP are being used in increasing quantities in products ranging from antibacterial coatings to additives in fuel. It is estimated that TiO_2 and SiO_2 NP are already produced worldwide at rates exceeding 1000 tons a year.(Piccinno *et al.*, 2012) Currently, the Woodrow Wilson database lists more than 1300 consumer products where NP are used. This number is only a conservative estimate, since the list contains only products that are identified as ''nano'' by the manufacturers themselves. As NP are becoming ubiquitous, significant amounts of them will unavoidably be released into the environment, (Hansen *et al.*, 2008) and many customers and workers may be at risk of becoming exposed to NP that have a high propensity to cross biological membranes and that are too small to be efficiently cleared by phagocytosis. (Buzea *et al.*, 2007) Consequently, with the disastrous use of asbestos still fresh in the memory, concerns have been raised regarding the safety of manufactured nanomaterials. (Handy *et al.*, 2008)

1.2. THE NEED FOR NUMBER-BASED NP CHARACTERIZATION FOR ENVIRONMENTAL REGULATION

The regulatory needs involve a classification step, a hazard assessment program, exposure assessment and environmental surveillance programs which together form the basis for a risk assessment.

1.2.1. **Regulatory classification of nanomaterials**

The international standardization organization ISO definition of a NP is a particle having all dimensions below 100 nm. Currently NP fall mostly under the same regulatory framework as their constituent bulk materials. However, there is pressure for imposing more specific regulations based on particle size. The European commission has proposed a definition of a NM. It stipulates that for a product to be classified as a NM for regulatory assessments, 50 % of the particles by

number must have one or more dimensions below 100 nm. This applies also when the particles are part of larger aggregates. Enforcing legislation based on such definition demands validated methods and experimental procedures for measuring number based size distributions.(Ehara and Sakurai, 2010)

A number based size distribution (PSD) is the number of particles in a size class as a function of the particle diameter. Other common PSDs are *e.g.* mass, or scattered light intensity as a function of the diameter. The particle diameter is also a somewhat ambiguous concept because different techniques measure different physical properties such as projected areas (Electron microscopy), sedimentation coefficients, (Analytical ultracentrifugation) or diffusion coefficients (Dynamic light scattering). The diameters are expressed as equivalent spherical diameters (ESD). The ESD is the diameter of a sphere that would have the same properties, *e.g.* volume or diffusion coefficient, as the measured particles. Especially for non-spherical particles ESD measured by different techniques would differ substantially.

1.2.2. **Hazard testing**

NP are subject to the same standardized tests that were developed for conventional chemicals. However, in addition to chemical composition, NP are characterized by parameters such as size, shape, coating, and aggregation state (Hassellov *et al.*, 2008). Mass concentration is the only relevant dose metric for conventional chemicals. It might be sufficient for *e.g.* Ag NP that mainly act as sources of toxic metal ions (Fabrega *et al.*, 2011). The toxicity of many metal oxide particles is at least in part due to creation of reactive oxygen species (ROS) at their surfaces. (Nel *et al.*, 2006, Oberdorster *et al.*, 2007, Klaine *et al.*, 2008) In this case, the surface area is a more relevant measure of exposure. In all cases, the size and aggregation/agglomeration state is likely to play a key role, because the translocation within organism, surface area normalized reactivity, and solubility are dependent on these parameters. (Chithrani *et al.*, 2006, Chithrani and Chan, 2007)

The interpretation of toxicological data is thus a formidable task, requiring extensive characterization for meaningful interpretation of the results. There is therefore an ongoing debate of what is the minimum set of parameters that must be characterized to ensure reliability and comparability of studies. (Bouwmeester *et al.*, 2011), http://characterizationmatters.org/) The matter is further complicated, by that during a toxicity test NP may undergo transformation processes such as oxidation, dissolution, and agglomeration which raise demands

for monitoring the parameters of interest in the test media as a function of time. (Krug and Wick, 2011)

The needs in toxicological studies addressed in this thesis are including i) reliable methods for thorough physicochemical characterization (especially size determinations), and ii) rapid and simple minimum perturbing methods to measure size and particle number concentrations in water and solid matrices such as soil and sediments.

1.2.3. **Exposure assessment**

Exposure assessments comprise: i) emission sources quantified, e.g. as in the studies where TiO2 emitted from façade paint, and AgNPs emitted from sock fabrics and NP producing washing machine respectively were quantified (Benn and Westerhoff, 2008, Kaegi *et al.*, 2008, Farkas *et al.*, 2011). In such studies, the NP concentrations are quite high and the mixture of particles are not too complex.; ii) fate and transport studies (Battin *et al.*, 2009) also use relatively high concentrations, but have more complex sample matrices, and iii) validation of modeled predicted environmental concentrations. Here, ultra-trace concentrations need to be quantified against, complex backgrounds of natural and incidental NP in matrices such as waste water, soil, sediments or river water.

1.2.4. **Environmental surveillance**

As long as NP are suspected hazardous, their concentrations and transformation in the environment need to be monitored. (Paterson *et al.*, 2011) This requires development of selective and sensitive methods capable of quantification and characterization of trace level particle contamination in complex samples, such as waste water, road run-off, sediments and soil. In addition, human protection, food and feed crops, and drinking water all need to be subject of environmental surveillance programs.

Environmental material flow modeling and the analytical data that have accumulated so far predicts concentrations of NP to be roughly in the range 10^{-13} to 10^{-8} g/L for Ag, ZnO, TiO_2, and CeO_2 NP in surface waters and waste water treatment plant (WWTP) effluents. (Gottschalk. F, 2013) These results indicate also that NP are likely to become enriched in sediments and soils. The low concentrations are challenging the detection limits for sensitive elemental analysis techniques such as inductively coupled plasma mass spectrometry, ICP-MS or optical emission spectrometry, ICP-OES. Meanwhile, the concentrations of natural colloidal material (e.g. natural organic matter

(NOM), biological debris, FeOx, and silicate mineral debris) are orders of magnitude higher.

1.3. NUMBER BASED TECHNIQUES

1.3.1. **Measurement of size distributions and number concentrations of NP in dispersion with non-selective methods**

NP are too small for being imaged directly by visible light. The light scattered by them can however be detected and used for localizing them. This is used by optical particle counters, however these devices do not achieve close to 100 % counting efficiency for small particles. A more practical approach for nanoparticles is to place them under a microscope and illuminate them from the side using a strong light source.

During Nanoparticle tracking analysis (NTA), the particles are visualized by the light scattered from an illuminating laser beam. (Malloy and Carr, 2006) The diffusion coefficients are determined by tracking the particles' Brownian motion using video microscopy. The hydrodynamic diameters can be determined from the diffusion coefficients, and the c_p from the number of visible particles following calibration with a standard dispersion having a known number concentration.

For strongly scattering materials such as Au, it is possible to determine the c_p and PSD of particles as small as 10 nm, while particles of most other materials must be larger for the technique to be applicable. The method relies on complex interplay between light scattering from an anisotropic laser beam, particle tracking software, and user defined image processing parameters. (Malloy and Carr, 2006) Validation is thus difficult although expected results have been obtained for many samples. (Bootz *et al.*, 2004, Malloy and Carr, 2006)

Number concentrations and size distributions can also be obtained by techniques such as laser induced breakdown detection (LIBD) (Kim and Walther, 2007) and elctrospray scanning mobility particle sizer (ES-SMPS) (Cole *et al.*, 2009) combined with a condensation nucleus counter. The problem with the latter technique is that dissolved material precipitate on the particles or form new particles that interfere with the analysis. Laser induced breakdown detection (LIBD) is capable of sizing and quantifying colloidal particles at concentrations as low as 10^2 particles/mL. However data analysis algorithms restrict the measurement of size distributions to only a few size classes. The accuracy of c_p determination for both techniques relies on the calibration standards.

In addition to the aforementioned techniques, there are several emerging ones that have so far seen no, or only a limited number of applications. Polymer membranes with micrometer sized apertures have been used to create coulter counter type particle sizers where particles restrain the ionic conductivity as they cross the membrane. (Scanning ion occlusion sensing, SIOS) (Vogel *et al.*, 2011) Measurement of number concentrations without calibration is possible. (Roberts *et al.*, 2012) Commercially available instruments such as Qnano are capable of measuring particle sizes down to 50 nm. In suspended nano channel resonator (SNR) devices, particles are transported in micro fluidic channels across an oscillating cantilever. The particles induce a frequency shift proportional to their buoyant mass. Calibration is readily done using fluids of known density. A SNR with improved mass resolution was used to measure accurately the size distribution of 50 nm, and detect 20 nm Au NP. (Lee *et al.*, 2010) None of these emerging techniques was applied in this thesis.

1.3.2. **Electron microscopy**

A vast amount of transmission electron microscopy (TEM) work on environmental particles has been done through the years and have contributed to the insights of the important role of natural nanoparticles for *e.g.* contaminant transport and element cycling, (Hochella *et al.*, 2008) and fate of Ag NP in WWTP. (Kim *et al.*, 2010, Kaegi *et al.*, 2011) TEM facilitates imaging with sub-Å resolution, but the technique has limitations, since water containing samples may not be directly analyzed by standard instruments. Therefore, elaborate sample preparation often needs to be done which may lead to a loss of a fraction of the NP. Furthermore, only small volumes can be analyzed. When only trace amounts of the particles of interest are present in the sample, it is thus difficult to locate them and obtaining reliable statistical information.

Scanning electron microscopy (SEM) is capable of characterizing bulk samples with a few nanometer resolutions. The need for the samples to be electrically conductive may be overcome by applying a metal or carbon coating or using variable pressure, or environmental scanning electron microscopy (ESEM). Particles consisting of heavy elements are readily located using backscattered electron imaging which gives atomic number contrast. (Goldstein *et al.*, 2003)

Although SEM has less stringent requirements for sample preparation than TEM, most of the water content will evaporate at the low pressures in the sample chamber. Therefore e.g. biological tissues may require elaborate sample preparation procedures.

It is thus clear that sample preparation techniques need to be developed to allow making full use of the potential of electron microscopy techniques to analyze NP in complex samples. It is, however, expected that only relatively high number concentrations of NP can be analyzed using these techniques given the requirement of statistically significant counts.

Atomic force microscopy lacks specificity and cannot be combined with spectroscopic techniques such as EDX. It was therefore not considered for this study.

1.3.3. **Single particle ICP-MS**

Most work trying to asses NP concentrations in liquid samples have separated size fractions by filtration and then measured the concentrations of the elements of interest by methods such as ICP-MS or ICP-OES. Methods have also been developed for isolating the particles by extraction procedures. (Hartmann *et al.*, 2013, Hartmann and Schuster, 2013, Majedi *et al.*, 2013) More detailed analysis can be performed by combining ICP-MS or ICP-OES with field flow fractionation or hydrodynamic chromatography, (Dubascoux *et al.*, 2010) where, elemental concentrations are obtained as a function of particle diameter. However, it is known that a significant fraction of many elements are adsorbed on natural NP. The colloidal fraction of *e.g.* V and Pb has shown to be preferentially adsorbed on iron oxide particles, (Stolpe *et al.*, 2005) while *e.g.* are Cu, Ni and U are preferentially adsorbed on NOM. (Stolpe and Hassellöv, 2007) None of the mentioned techniques can thus distinguish particles of *e.g* TiO_2, metallic Ag, or CeO_2 from natural NP carrying their constituent elements.

The degree of specificity can be increased by using single particle ICP-MS (spICP-MS) developed by Degueldre *et. al.* (Degueldre, 2003, Degueldre, 2004, Degueldre, 2004, Degueldre, 2006, Degueldre, 2006) The ion plumes coming from individual particles vaporized and atomized in the plasma can be detected as outliers in the continuous signal originating from dissolved analyte by using short enough acquisition times (< 20 ms). The frequency of particle-related spikes are related to their number concentration while their intensities are proportional to the mass of analyte in the particles. The ICP-MS instrument can thus be used as an element-specific particle counter Moreover, particles consisting of the element of interest can be distinguished from the large numbers of particles with only a minuscule amount of analyte adsorbed on their surface.

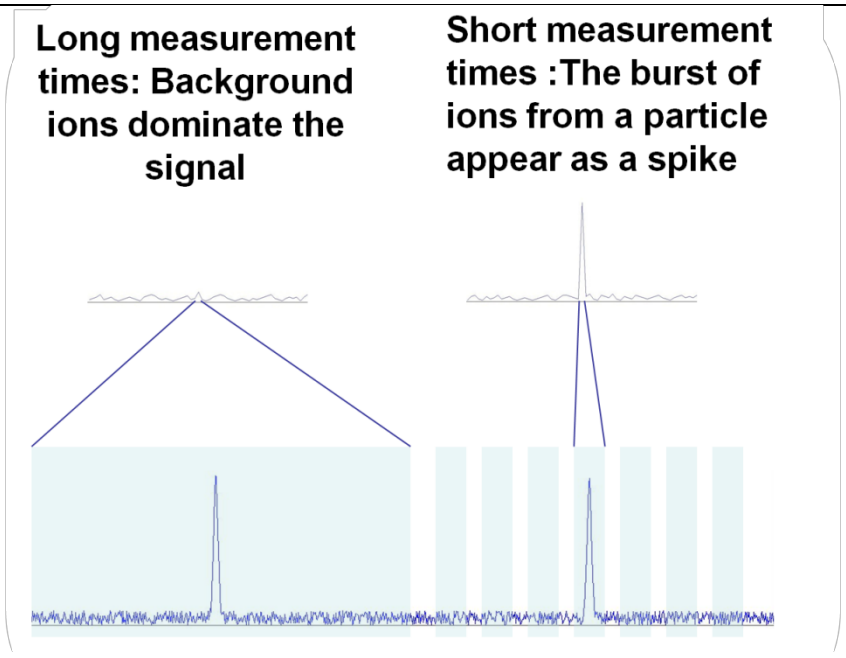

Figure 1 *Signals and data acquisition in conventional (left) and single particle ICP-MS (right).*

1.4. AIM

To develop methods for measuring number concentrations and size distributions in aqueous and solid environmental matrices which are sensitive and selective on a single particle level.

1.5. SPECIFIC OBJECTIVES AND APPROACHES

The working hypothesis has been that electron microscopy methods are important trace particle characterization methods due to the wealth of information that both scanning and transmission electron microscopy can provide on individual particles. Therefore one of the objectives is to explore and develop high contrast modes for certain particle compositions. Still, to analyze enough number of particles to obtain statistically validity with microscopy techniques is not practically feasible for environmental samples. Therefore another objective has been to develop quantitative methods that can determine size and number concentration. Nanoparticle Tracking Analysis was an emerging technique during this work that although not being able to chemically differentiate different NP, had interesting features (minimum perturbation, analysis speed and ease, sensitivity) warranting further investigations. Single particle ICP-MS was the most promising technique and most effort was dedicated to further develop this technique due to the analytical merits single particle chemical selectivity, highly sensitive and minimum perturbation.

The work was directed towards experimental validation of each of the methods followed by applications on environmental samples.

2. METHODS

2.1. NANOPARTICLE TRACKING ANALYSIS.

The resolution of optical microscopes is limited to ~200 nm by Airy diffraction. However, particles smaller than the diffraction limit can be visualized if illuminated by a strong light source located in a plane normal to the optical axis of the microscope. The particles scatter the light and appear as bright spots in the microscope. It is not possible to use the scattered light for imaging the dimensions or morphology of the particles. However, it is possible to obtain useful information, because the number of particles visible at a given moment is proportional to the particle number concentration (c_p). Furthermore, the particles undergo Brownian motion, and tracking the movement of a particle during a period of time allows determining its diffusion coefficient, and therefore hydrodynamic diameter, based on the Stokes-Einstein relation. This principle is used by nanoparticle tracking analysis (NTA). (Malloy and Carr, 2006)

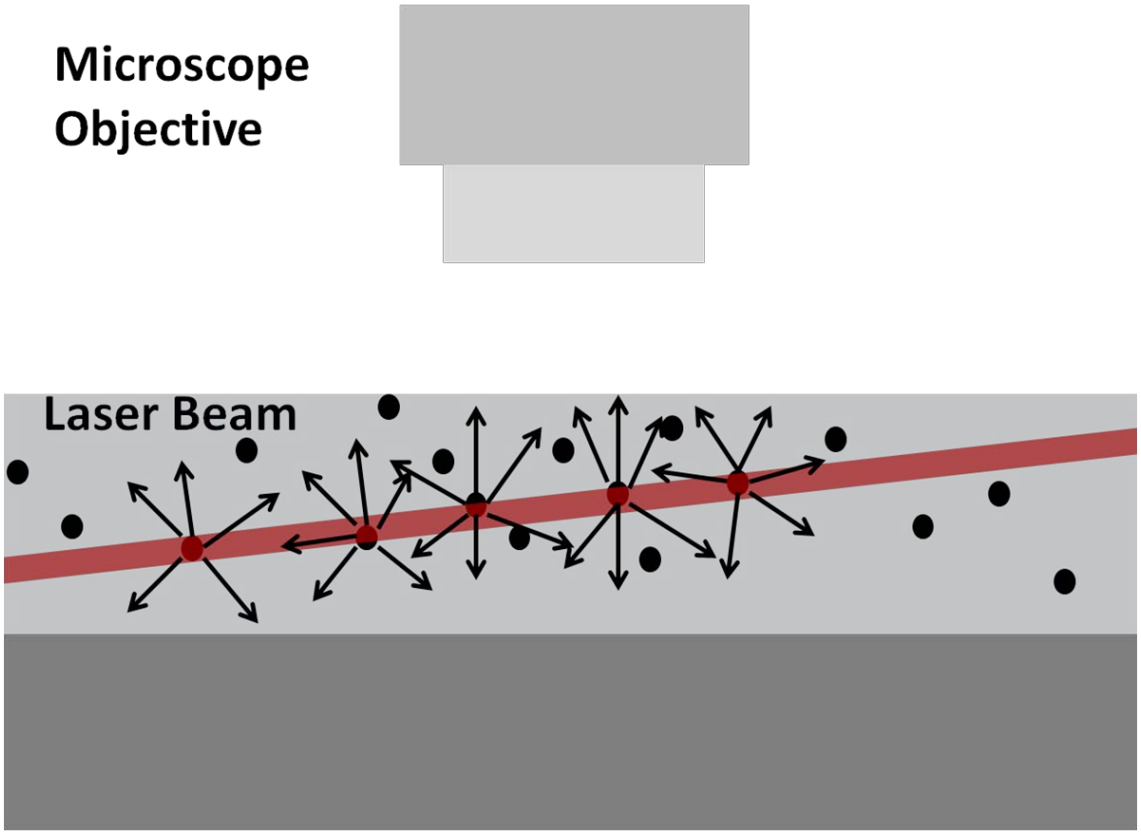

***Figure 2** Principles of NTA*

The Nanosight LM10 instrument that was used in this work illuminates the particles in a 0.3 mL sample chamber with a 40 mW 638 nm continuous laser (Figure 2). The particles in the holder were

observed through a glass window by a microscope. The size range where the technique is applicable is dependent on the refractive indesx of the particles. It is possible to visualize considerable smaller particles of *e.g* gold, which provides strong refractive index contrast against water compared to for instance polymer latexes. A camera connected to the microscope was used to capture videos at a rate of 30 frames s^{-1}.The particles are identified and tracked from frame to frame and their diffusion coefficients, D_s are determined from their mean squared displacements in the x, and y direction during a time t in the image plane.

$$\overline{x^2} + \overline{y^2} = 4Dt \qquad (1)$$

The hydrodynamic diameter, d_h can be calculated from the Stokes-Einstein equation:

$$\frac{3\pi\eta D}{k_b T} = d_h \qquad (2)$$

Where η is viscosity, k_b is the Boltzmann constant, and T is the temperature. As a consequence of that the particles are only tracked in two dimensions, the diffusion coefficient is more often under, than overestimated because movement in the z-direction is not taken into account. This causes bias towards larger particles that manifests itself as a "tail" of large particles. In addition, measurements of polydisperse samples might be compromised by greater light spots from larger particles obscuring those of the smaller ones. Another source of uncertainty is that the particles are not always tracked through enough frames to produce a statistically valid estimate of the diffusion coefficient.

The c_p can be determined from the average number of particles that on each moment are visible and identified as such. However, this requires calibration with a number concentration standard. The smaller fast diffusing particles may enter and exit the volume where the particles are observed (detection volume) more frequently, increasing their apparent concentration. However, this effect is corrected for in the software.

The analysis is also dependent on a number of image analysis and tracking parameters set by the user. This introduces component of subjectivity to the analysis. Although accurate sizing of particle standards and polydisperse mixtures of these have been reported , NTA

is still an emerging technique for which all sources of bias have not yet been identified or quantified. Therefore, the results obtained by NTA must be interpreted with care and on a sample to sample basis.

In this work, the applicability of NTA for determining number concentrations and size distributions was evaluated both for simple dispersions (Paper I, III, and IV) and environmental colloids (Paper I). The laser illumination is not homogenous. The intensity profile of the beam is presumably Gaussian with the illumination being most intense in its centre. It is known that larger, strongly scattering particles may be visualized further out on the beam edges than weak scatterers, which thus give a size and material dependence on the effective optical volume. This may skew size distributions and introduce material dependency on the sensitivity with respect to c_p. A mathematical model was therefore developed for the dependency of sensitivity of the particles scattering power (Paper II, and III). Particles of stronger scattering materials produce brighter light spots. A test of using this feature for detecting Au particles spiked into juice was carried out in paper II.

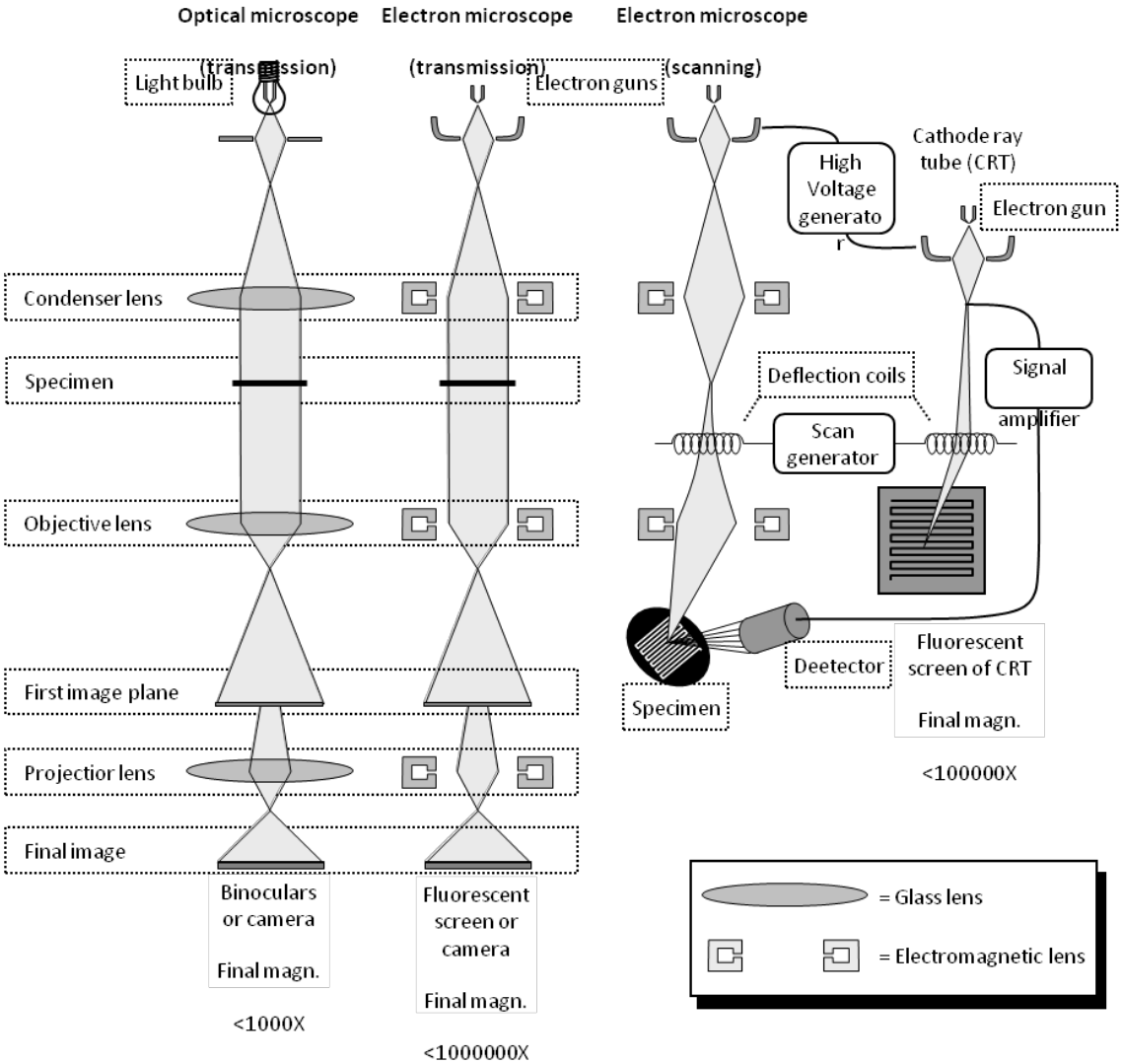

***Figure 3** Principles of electron microscopy compared to optical microscopy*

2.2. TEM

In TEM, the wave properties of high kinetic energy electrons are used for imaging samples in a fashion analogous to the optical microscope (Figure 3). Typically, 200 kV acceleration voltages are used which allow sub nanometer resolution. Combined with elemental analysis techniques such as energy dispersive x-Ray spectroscopy (EDX), energy filtered imaging (EFTEM) and crystal structure analysis by acquiring selected area electron diffractograms (SAED), or by Fourier transforming selected parts of the images, TEM has a tremendous potential for characterization of individual NP (Figure 4).

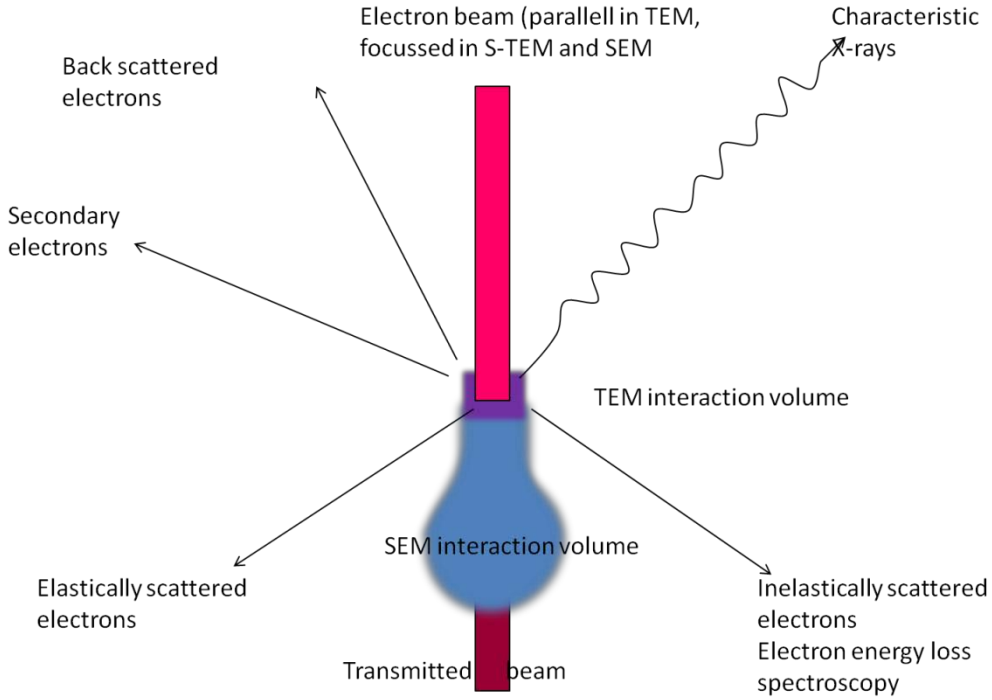

***Figure 4** Spectroscopic signals used for Analytical electron microscopy*

To analyse particles they need to be transferred to metal grids coated with a thin carbon film or SiN layer. (TEM grids) The most common way of preparing simple dispersions is to place a droplet of sample on a holey carbon grid (TEM grid coated with a perforated carbon film). The perforated carbon grids are less prone to rupture upon drying than solid films. More elaborate schemes for preparing environmental samples for microscopy analysis have been developed for aqueous dispersions based on centrifugation, (Nomizu and Mizuike, 1986) or embedding the particles in resin. (Hochella *et al.*, 1999) Airborne particles have been analysed after transferring them from filters to TEM grids, (Utsunomiya and Ewing, 2003, Utsunomiya *et al.*, 2004) Even methods for extracting heavy metal containing fractions from sediments have been developed. (Plathe *et al.*, 2013). However, these methods have limitations when the goal is to analyze NP. When only trace amounts of the particles of

interest are present in the sample, it is difficult to locate them, let alone that a statistically significant number of them can be counted. Even when present in ample amounts characterization of a significant number of particles is time consuming. In addition, it is difficult to obtain quantitative information because the transferring of particles to TEM grids is not always fully quantitative.

While the occurrence of sample preparation artifacts are commonly recognized for complex samples, (Mavrocordatos *et al.*, 2007) TEM is commonly employed for PSD measurement without considering the possibility of bias. Here, the reliability of the commonly used drop-cast method with holey carbon grids is put under scrutiny in the method comparison study in paper III.

TEM is also used for characterization of tungsten containing particles in paper VIII. Here, the problem of low concentrations was partially overcome by preconcentrating the colloids in the road runoff water sample by continuous flow ultrafiltration.

2.3. SCANNING ELECTRON MICROSCOPY.

In scanning electron microscopy (SEM) (Figure 3), (Goldstein *et al.*, 2003) the sample is probed by a focused electron beam that is scanned across the sample surface in a raster fashion. The beam is accelerated through a potential difference, typically ranging from a few hundred volts up to 30 kV. When entering the sample, the electron beam spreads into a pear shaped interaction volume reaching several microns under the surface. One probes the electrons leaving the sample or X-rays produced as a result of the interaction between the electron beam and the sample (Figure 4). Part of the electrons return to the surface of the sample after undergoing multiple elastic scattering events (backscattered electrons, BSE). X-rays and secondary electrons (SE) are produced following excitation processes due to inelastic scattering. The BSE may leave the sample while maintaining a large fraction of their incident kinetic energies while the kinetic energies of SE are typically only a few eV. The image is built up by measuring the BSE or SE emission point by point in a raster scan over the specimen.

Secondary electrons were in this work measured by the Everhart Thornley detector. The detector consists of a scintillator surrounded by a Faraday cage. A positive bias (<250 V) is applied on the Faraday cage to attract SE. The faraday cage also acts to prevent the electron beam from being distorted by the voltage of 10-12 kV applied on the scintillator that accelerates the SE to high enough kinetic energies to produce light upon hitting the scintillator. The light is lead out from the

sample chamber to a photomultiplier tube by a total internal reflection wave guide. Backscattered electrons are not screened but contribute to the signal. Both the BSE emitted at solid angles covered by the scintillator, and secondary electrons emitted due to BSE striking the sample chamber walls are detected. The resulting image is therefore due to a combination of SE and BSE.

Secondary electron imaging gives contrast based mainly on topography. The technique is surface sensitive since only the SE originating from the topmost few nanometers of the sample are able to reach and escape from the surface. The secondary electron coefficient, δ is defined as the current of secondary electrons emitted from the sample divided by the current of the incident beam. It approximately depends on the surface tilt angle, θ as follows.

$$\delta=\delta_0/\cos(\theta) \qquad (3)$$

The δ_0 is the SE coefficient of a surface parallel to the normal of the incident beam. The resulting image can with a good approximation be interpreted as an optical image of the surface, illuminated by a light source located at the detector.

BSE were measured with a solid state detector. The electrons strike a semiconductor chip with a p-n junction under reverse bias. A large number of electron hole pairs are produced, and the resulting current through the detector is further amplified to produce the signal used for the image. The side facing the sample is coated with a thin gold layer which the low energy SE cannot pass so that the BSE are probed specifically in this case.

BSE imaging is useful for finding heavy metal containing particles against a background consisting of light elements. The contrast in BSE images arises from a superposition of density and topography. The fraction of the incident beam current that is backscattered from the sample, η increases with average atomic number Z, and θ according to the Arnal equation as:

$$\eta=1/(1+\cos\theta)^{9/Z} \qquad (4)$$

To interpret BSE images one has to consider that the backscattered electrons may convey information about structures located at several microns depth from the surface. The resulting image can be compared with an optical image of a partially transparent object.

X-rays are emitted when the electron beam excites atoms in the sample. X-rays are produced when these atoms return to their ground

state. The X-rays were detected by an energy dispersive detector. Here the incident X-ray photons induce pulses of current through a detector consisting of a PIN diode under a negative bias of around 1 kV. The detector is cooled with liquid nitrogen to achieve sufficiently low conductivity. When X-ray photons strike the diode they produce a number of electron-hole pairs in the intrinsic layer that give rise to a current spike. Individual photons are counted as the detector is connected to a pulse counting circuit. The intensity of the current spikes are proportional to the energy of the X-ray photons.

Energy dispersive X-ray (EDX) spectroscopy can be used to confirm the elemental content of the found particles. However, the intensities of the element specific X-ray lines depend, besides concentration, on the chemical composition and topography of the sample. Because it is for quantitative analysis assumed that the surface is flat and the sample is homogenous within the interaction volume, the technique is not fully quantitative for small particles.

Imaging of insulating samples is difficult because the electrons in the incident beam must be conducted away from the sample to avoid artifacts due to build up of charge. If the sample is charged, the electron beam becomes deflected from the intended scan pattern. This often shows up as white streaks in the image. Variable pressure or environmental SEM (VP-SEM or ESEM, respectively) allows keeping a higher pressure in the sample chamber than what is required in the electron gun. This is achieved by introducing a gas into the sample chamber. The gas is ionized along the path of the electron beam and the positively charged molecules created are attracted to any negatively charged areas of the sample surface, thereby neutralizing excess surface charges. In this way, imaging of non-conducting samples becomes possible. However, this comes at the expense of a slightly poorer resolution, because the electron beam spreads due to collisions with the molecules in the air.

Almost any type of sample can be characterized as long as it fits in the sample chamber, but drying artifacts will be encountered for wet samples. (Dudkiewicz *et al.*, 2011) It was found that for samples of very low conductivity such as soil and road dust, a good compromise between sufficient resolution and suppression of charging effects was obtained when the chamber pressure was held at 0.5-0.6 Torr.

Both imaging and sample preparation has been extensively studied. However, despite that complicated sample preparation is not necessary and the number of particles visible in the images can be expected to be proportional to their concentration very little work has been done on

developing quantitative analysis of NP in solid matrices. If it is known how deep in the matrix particles can be detected, the sampling depth, it is possible to calculate the number of particles per volume from the number of particles detected per imaged area.

An attempt to quantify the number of precipitates in steel was made by Korcakova *et al*. (2001) using the Kanaya Okayama electron range combined with an expression for from how deep in the matrix backscattered electrons are emitted. (Kanaya and Okayama, 1972) This approach was adapted for complex soil matrices was made in paper IV. In addition, the possibility to calibrate for the sampling depth by spiking the soil with dispersions of known concentration was investigated. The accuracy of sizing particles dispersed in soil was also evaluated.

It was mentioned that X-ray spectroscopy of particulate matter is not fully quantitative. However, by using the characteristic X-rays for imaging, maps of the relative abundance of elements in different locations can be constructed. This EDX mapping was used for identification of tungsten containing phases found in road dust.

2.4. INDUCTIVELY COUPLED PLASMA-MASS SPECTROMETRY.

ICP-MS is a technique for measuring elemental concentrations in liquid samples. A Thermo-Finnigan element 2 sector field instrument was used in this work. The technique is highly sensitive (typical detection limits ng/L to pg/L), and for isotopes for which there are no interfering species originating from the plasma, the detection limits are set by the contamination levels of reagents and laboratory as well as sample introduction components rather than the capabilities of the instrument. A overview of the instrument is shown in Figure 5.

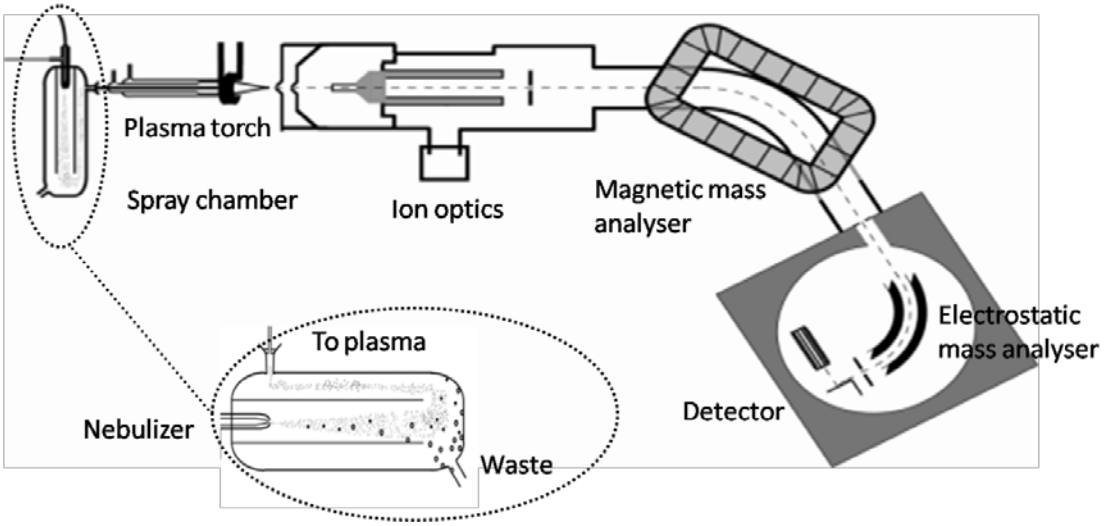

Figure 5 *Overview over the components of ICP-MS instrument.*

The sample is first pumped into a nebulizer that produces an aerosol. In the subsequent step, the larger droplets are removed in the spray chamber. A small fraction of the sample (~1-25 %) containing the finest droplets with diameters mostly below 10 μm enter a plasma torch where the sample is atomized and partially ionized at temperatures reaching up to 10 000 K. The ions are extracted from the plasma and focused to a beam by a system of electrostatic lenses.

The ion beam is accelerated through the flight tube by a 20 kV voltage. The tube is curved, and only the ions having the chosen mass to charge ratio are allowed to pass to the detector by bending their trajectories by magnetic and electrostatic fields. The ions strike a dynode conversion plate which emits electrons that are amplified in the secondary electron multiplier detector that is connected to a pulse counting circuit counting individual ions. For high count rates, the analog current flowing through the electron multiplier is measured instead to obtain a very high linear dynamic range over 9 orders of magnitude.

2.5. SINGLE PARTICLE ICP-MS

2.5.1. **Background**

Nomizu *et al.* (2002) evaluated ICP-MS for analysis of individual artificially generated Zn acetate aerosol particles. The particles entering the plasma produced ion bursts with a duration of a few tenths of a millisecond of which the Zn content could be detected and integrated using a secondary electron multiplier connected to an oscilloscope. Single particle ICP-MS for liquid particle dispersions was introduced by Degueldre *et al.* (2006). These authors and later Laborda *et al.* (2011) could establish that the bursts of ions produced by individual particles are possible to detect as outliers in the trace of ICP-MS signal *vs.* time using conventional instrumentation and sample introduction systems. The frequencies of such pulses are proportional to their number concentration, while the pulse intensities is proportional to the mass of analyte contained in each particle. The particles volume equivalent spherical diameters can thus be determined, provided that the spike intensities have been calibrated for analyte mass, and the chemical composition is known. Therefore spICP-MS has the potential to be developed into a powerful technique for trace particle analysis. In the following chapters the nature of the ion bursts, and the measurement of them are first reviewed, followed by the basics of particle counting and sizing that were developed previously (Degueldre and Favarger, 2003, Laborda *et al.*, 2011) and in paper VI.

Measurement of particle events. The signal in a data point, also called dwell, is acquired by counting the ions during a period called the dwell time, t_{dwell}. Most data in this thesis there were acquired by having a few ms time gap between the dwells (Figure 1). It appeared that it is possible to acquire dwells even without any time spacing on the element 2 ICP-MS. However, this mode of acquisition was used only as a feasibility study for measuring a few AgNP in paper V with a time resolution of 0.1 ms.

In each dwell, the signal (ion count) is due to the sum of ions originating from the dissolved background and the occasional particle events. The number of ions due to dissolved analyte that arrive at detector during a dwell, I_{diss} is given by $t_{dwell}*k_{diss}$ where k_{diss} is the count rate (counts s^{-1}) due to dissolved analyte. The ratio, R, between the particle event, I_{part} and dissolved signals, I_{diss} is thus given by:

$$R = 1 + \frac{I_{part}}{t_{dwell}\, k_{diss}} \qquad (5)$$

Equation (5) suggests shortening t_{dwell} will improve R by decreasing the numbers of dissolved ions measured during each dwell. I_{part} is not affected by shortening t_{dwell} provided that all ions contained in the particle evens arrive within one dwell. Typically, t_{dwell} < 20 ms are used for spICP-MS, whereas longer dwell times (> 100 ms) are used in conventional ICP-MS to obtain stable average signals.

2.5.2. **Particle events**

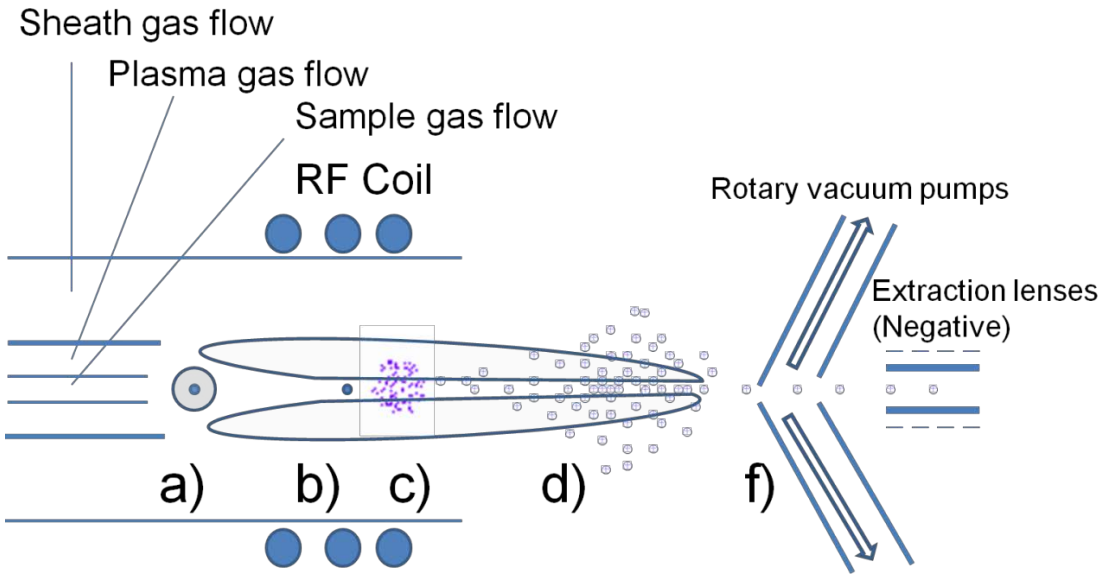

Figure 6 *The processes occurring upon ionization and atomization of particles in the plasma.*

The processes occuring upon atomization an ionization of small particles in plasma is unlikely much different from that of dissolved analytes. In fact, dissolved analytes are atomized from the solid particles that remain after evaporation of the carrying droplet. The studies on fate of single droplets carrying dissolved analyte using e.g. time gated optical emission and saturated laser induced fluorescence, (Dziewatkoski *et al.*, 1996, Olesik *et al.*, 1997, Stewart and Olesik, 1999) high speed photography, (Winge *et al.*, 1991, Houk *et al.*, 1997) and computer simulations (Horner *et al.*, 2002, Horner *et al.*, 2008) are therefore useful for understanding the particle events as well.

In Figure 6 is shown how: a) a droplet carrying a particle enters the plasma and starts to vaporize. The location in the plasma where the solvent is completely vaporized varies and is closer to the torch with higher plasma temperature, lower carrier gas flow rate but particularly with smaller droplet size. b) Once the solvent has evaporated, the vaporization of the particle and the subsequent ionization are relatively fast processes, at most 0.1-0.15 ms. c) The cloud of ions expands due to diffusion while it is transported by the gas flow to the sampler cone orifice. d) The duration of the ion burst eventually measured at the detector is greatly affected by the speed and dimensions of the ion cloud at the sampler cone orifice. A model has been developed and experimentally verified, (Dziewatkoski *et al.*, 1996) where the analyte concentration at sampler cone, C and therefore signal intensity as a function of time, t measured by the detector depends on the distance to the point of vaporization of the particle, y', the speed of the sample gas stream in the plasma, v and the diffusion coefficient D_{ion} of the ions:

$$C=\frac{C_0}{(8\pi D_{ion})^{3/2}} e^{\frac{-(y'-vt)^2}{4D_{ion}t}} \qquad (6)$$

C_0 is the background level. Equation (6) suggests if the plasma is stable and sample gas flow is constant, the only source of variation in C is the point of vaporization. Varying droplet sizes result therefore in noise in particle signals and some studies have therefore used monodisperse dried microparticle injectors (MDMI) to minimize the variation in droplet size and thus noise on the particle signal. (Gschwind *et al.*, 2011, Gschwind *et al.*, 2013)

2.5.3. **Measurement of particle diameter**

The number of ions of dissolved, I_{diss}, or particle bound analytes, I_{part} arriving at the detector in each dwell is given by (see paper VI):

$$I_{diss} = t_{dwell} f_{neb} c_{diss} A q \times f_{is} f_{ion} f_{plasma} f_{trans}$$

$$I_{part} = m_{part} AM^{-1} \times f_{is} f_{ion} f_{plasma} f_{trans} \quad (7)$$

Both the equation for dissolved signals and the equation for particle bound signals consist of two parts that account for the number of analyte atoms introduced to the plasma, and efficiency factors in the plasma and mass spectrometer respectively. The first part of the equation for dissolved signal gives the number of dissolved analyte atoms introduced to the plasma, a number that is related to the analyte concentration c_{diss} (mol L^{-1}) by the nebulization efficiency, f_{neb}, i.e. the fraction of the analyte that passes through the nebulizer and spray chamber. A is Avogadro's number, q is the flow rate of sample into the nebulizer in Ls^{-1}. The first part of the equation for particle bound signals consists of the mass of analyte contained in the particle, m_{part} (g) and the molar mass of the analyte (g mol^{-1}).

The second parts of the equations (7) express the detection efficiency or the fractions of analyte atoms entering the plasma that are actually detected. f_{is} is the abundance of the monitored isotope, f_{ion} the fraction of analyte that becomes singly charged positive ions in the plasma, f_{plasma} the fraction of analyte exiting the plasma through the sampler cone, and f_{trans} is the transport efficiency or the fraction of ions that is transported through the mass spectrometer from the sampler cone to the detector. The detection efficiency is likely equal for dissolved ad particle bound analytes because several studies have shown that there is no significant difference between conventional ICP-MS analysis of acid digested or non-digested Au and Ag nanoparticles smaller than 100 nm diameter (Allabashi *et al.*, 2009, Mitrano *et al.*, 2012) and the m_{part} of silica particles measured by spICP-MS agrees with the values calculated from particle diameter for up to 800 nm particles. (Olesik and Gray, 2012)

2.5.4. **spICP-MS size distributions**

The process of calculating size distribution from the signals is illustrated in Figure 6. The detection efficiency can be determined from a plot of signal intensity against the amount of dissolved analyte that enters the plasma during each dwell. This requires that f_{neb} is known. Measuring f_{neb} accurately is thus crucial for both correct sizing and particle number determination with spICP-MS, as discussed further. m_{part} in equation (7) can be determined from I_{part} by using information from the calibration curve:

$$m_{part} = \frac{I_{part} - r}{S_i} \qquad (8)$$

where r is the recipient of the calibration curve, and S_i is the sensitivity or calibration curve slope in counts g^{-1}. If the density of the measured element in the particles, ρ is known, the volume equivalent spherical diameters, d_{part} can then be calculated from:

$$d_{part} = 2 \sqrt[3]{\frac{m_{part}}{\frac{4}{3}\pi\rho}} \qquad (9)$$

After converting mass to diameter using equation (9), the originally constant bin width in the frequency-intensity histogram now increases with particle size. The particle count in each bin is divided by the bin width to produce a size distribution based on a normalized frequency; particles/nm as a function of particle diameter in nm.

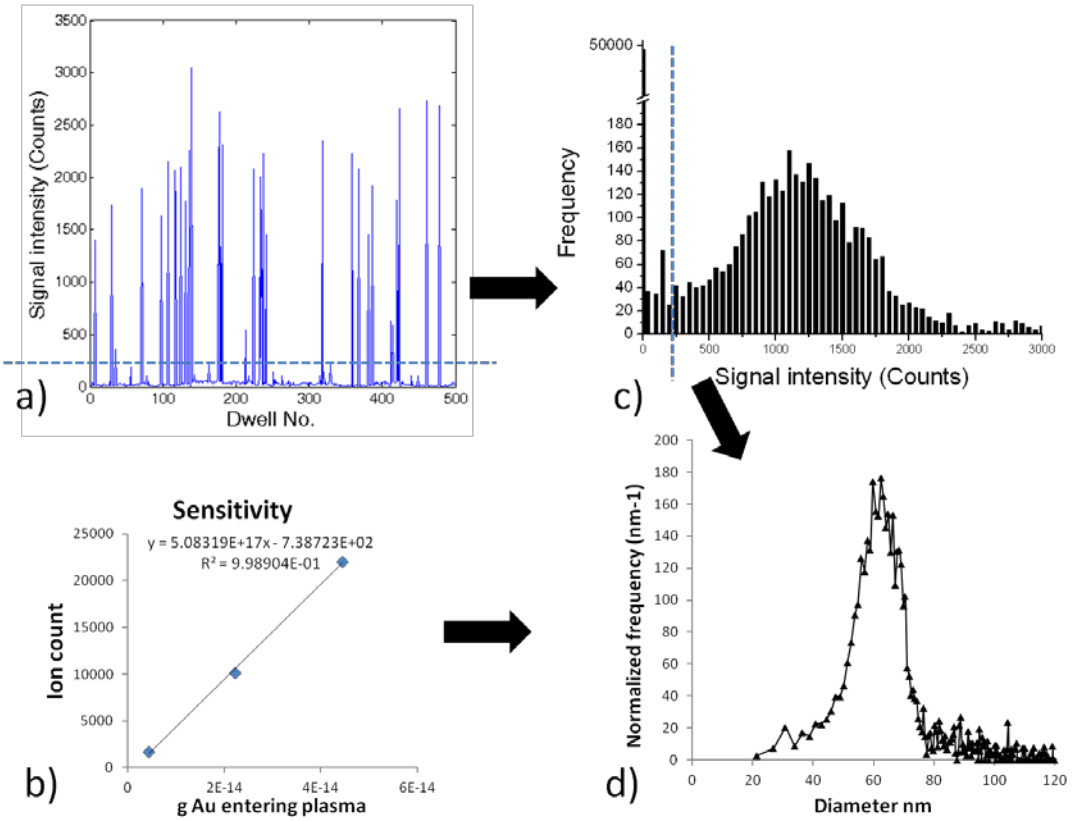

Figure 6 *Calculation of spICP-MS size distribution from raw data.* ***a)*** *The signal intensity of a sequence of dwells. The spikes are due to particles while the continuous signal originates from dissolved analyte. The horizontal line is the detection threshold. The dwells having signal intensities above the detection threshold are considered to contain particle events. The determination of detection thresholds is discussed in paper VI* ***b)*** *A calibration curve of the signal intensity against the mass of analyte entering plasma. Such plots provide the parameters to equation 8.* ***c)*** *The data shown in* ***a)*** *is replotted to a frequency intensity diagram. The mean level of the dissolved background signal is subtracted from the data points containing particle signals and the particle diameters are calculated from the ion count using equations 8, and 9.*

The size detection limit, DL_s, which is the smallest particle that is possible to detect accurately, is determined by the noise levels of the dissolved background signal as discussed in paper VI. The size distributions are in some extent broadened by noise in particle signals. An assessment of sources and magnitudes of noise was made in paper V.

2.5.5. **Determining nebulization efficiency**

Unless stated otherwise the f_{neb} was measured using the waste collection (WC) method. (Smith and Browner, 1982) Here, the inflow to the nebulizer is monitored by a flow meter, while the flow through spray chamber waste outlet is monitored by collecting waste and weighing it at regular intervals. The difference between these flows is assumed to have entered the plasma. Only the smallest droplets having the largest specific surface area enters the plasma. Because analyte is depleted from droplet surfaces, analyte is redistributed from the plasma to the waste flow. (Borowiec *et al.*, 1980) Therefore, the concentration ratio between analyte in nebulizer and waste flows must be measured for most accurate results.

Other methods to determine fneb or alternative approaches have been developed as well. The f_{neb} can also be measured by adjusting it so that spICP-MS reproduces the PSD of reference particles such as NIST gold NPs or the particles can be counted in dispersion with known c_p. (Pace *et al.*, 2011)

When sample is introduced by an MDMI device, the size calibration is based on the known size and concentration in the droplet and determinging f_{neb} is no longer needed. However, by using this method one faces the analogous problem of determining the droplet size accurately. (Gschwind *et al.*, 2011) When using direct injection nebulizers (DIN or DIHEN), the whole nebulizer flow is directed to plasma ($f_{\mathrm{neb}} = 1$). However a large fraction of the sample introduced by these devices does not contribute to the measurements because the droplets follow trajectories that are not lying on the sampler cone axis.(Jorabchi *et al.*, 2005)

To validate the f_{neb} measurements, PSDs of Au and Ag NP were in paper V compared with PSD measured by SEM. The role of other error sources in spICP-MS, such as particle events that are measured only partially because they are not fully coinciding with a dwell, and the need for proper correction of detector dead time are also discussed.

2.5.6. **Determining number concentrations**

The number of particles that on average enters the plasma during a dwell depends on c_p as:

$$\lambda = q f_{neb} c_p t_{dwell} \qquad (10)$$

If the particles arrive randomly, the number of single, i.e. when the ion cloud from only one particle arrives during a dwell, and multiple (k) particle events, i.e. when more than one ion cloud arrives, is given by the Poisson distribution

$$p_k = e^{-\lambda}\lambda^k/k! \qquad \text{k= 1, 2, 3 ...} \qquad (11)$$

The probability of obtaining a particle event, p_p, is obtained by summing the k-particle events.

$$p_p = \sum_{n=1}^{n=\infty} p_k \qquad \text{n=1, 2, 3...} \qquad (12)$$

For low frequencies of particle events, p_p is approximately equal to λ, in which case the number of particles counted in a sequence of D dwells depends on c_p as:

$$\frac{N}{D q f_{neb} t_{dwell}} = c_p \qquad (13)$$

The measurement of c_p is thus also relying on determination of f_{neb}. A typical nebulizer-spray chamber system allows ~ 0.05- 0.1 mL of sample into the plasma each minute. Therefore, the particles in several mL of sample can be counted in a measurement session which allows quantification of extremely low NP concentrations.

spICP-MS is validated for measurement of c_p in paper V, where also the role of counting statistics is discussed. Distinguishing the particle events from dissolved signals is not trivial when the particle events are scarce, or have a low intensity relative to the dissolved signals. Therefore an outlier detection algorithm was evaluated in paper VI for quantification of trace level concentrations.

spICP-MS was used for characterizing particles in a number of environmental samples including effluent from a Ag NP producing washing machine (Paper VII), treated WWTP effluent(Paper VI), and road runoff (Paper VIII).

3. RESULTS AND DISCUSSION

3.1. COMPARISON OF PARTICLE SIZING TECHNIQUES FOR SILICA NP

The results from measuring the size and size distribution of colloidal silica particles with NTA, TEM, SEM, ES-SMPS, DLS, and SedFFF hyphenated with DLS were compared in paper III to assess the accuracy, and to investigate material specific effects that affects the sizing of colloidal silica which is one of the technologically most important type of nanoparticles. The dispersion used for the method comparison was one of IRMM reference materials that had been evaluated for stability prior to our study. Since the objective was to investigate primary particle size resolution and precision, accuracy, and any potential instrumental bias, the high sphericity (average aspect ratio 1.08) was suitable. This means that differences arising solely from the geometry and method specific differences in the size measurands (e.g. different equivalent diameters measured) can be excluded. The concentration of aggregates was also very low, which avoided the influence of such on the measured primary particle size distribution. The mean diameters, and widths of the size distributions are listed in Table 1.

Table 1 *The mean and Z-average diameters, together with the width of the PSD obtained for sample A, and B with different methods. The uncertainty values are 95 % confidence intervals. The RSD value is the spread in particle diameters.*

Method	**d_{mode} (nm)**	**$d_{arithmetic\ mean}$ (nm)**	**$d_{harmonic\ Z\text{-}ave}$ (nm)**	**RSD (%)**
Sample A				
ES-SMPS (n=7)[b)]	36	33.9± 0.9	40.4 ± 1.4[a)]	15.8
SEM (n=1)	37	34.7 ± 1.74	39.1±2.0[a)]	17.7
TEM (n=1)	31	31.6 ± 1.6	n/a	17.1
DLS[c)]	n/a	n/a	36.5±0.3 (34.8)[d)]	n/a
sedFFF-DLS(n=3)	n/a	n/a	35.5±0.4	n/a
Sample B				
ES-SMPS (n=12)	36 ± 1	31.4± 1.0	41.0± 1.2[a)]	25.1
TEM (n=1)	30	31.0 ± 1.6	n/a	19.6
DLS[c]	n/a	n/a	37.3±0.3	n/a
NTA (n=1)	68	n/a	n/a	n/a

[a)] Calculated value.[b)] n equals the number of independent measurements. [c)] Determined by extrapolation to infinite dilution.[d)] Corrected for polydispersity effects

The comparison investigation resulted in following findings.

- The mean diameter obtained by TEM was 9 % smaller than that measured by SEM. Examination of identical particles in both microscopes ruled out inconsistent calibration of magnification, or the differing contrast mechanisms as the sole explanation for the discrepancy. The inaccurate sizing was therefore attributed to a sample preparation artifact. The hypothesis is that during sample preparation the dispersion flows through the perforated TEM grid, and a bias is created towards smaller particles since they have higher propensity to diffuse across the stream lines, and settle away from the holes, whereas larger particles tend follow the stream and become absorbed by the underlying Kleenex^{TM} tissue. These effects were also observed by Baalousha *et al.* (2012). For SEM, the whole particle population is retained on the Si wafer and no such bias is possible. Methods for preparing samples for TEM analysis without this bias should therefore be developed and validated.
- The collective diffusion coefficient, as measured by DLS, is expected to depend linearly on concentration. (Vandenbroeck *et al.*, 1981, Cichocki and Felderhof, 1988) To determine the hydrodynamic diameter by DLS, the diffusion coefficient is therefore measured at several concentrations, and extrapolated to infinite dilution assuming a linear dependence. It was, however, found that the concentration dependence deviates from linearity at low concentrations. This phenomenon has been observed earlier for TiO_2 and explained by the tendency of small particle to cluster around aggregates (Holmberg *et al.*, 2011). As aggregate concentrations as low as $1/10^6$ of the total particle concentration is enough to induce these effects, the behavior at very low concentration (< 0.1 wt %) should be investigated in order to ensure that only data in the linear region is used for the extrapolation procedure.
- Because the hydrodynamic diameter includes waters of hydration, one could expect that after correction for the different weightings of the size distributions, DLS diameters would be slightly larger than those measured by ES-SMPS, and SEM. Instead, DLS yielded smaller diameters, both for batch measurements on the whole particle population, and when it was first fractionated with sedFFF. There is evidence that a permeable gel layer forms on silica surfaces in contact with water, although this is still regarded controversial. The existence

of such gel layer could readily explain the anomalous results. The core particle shrinks when the SiO_2 chains protrude from the surface;(Vigil *et al.*, 1994) meanwhile the loose network of silica polymers is unable to retard diffusion. (Masliyah *et al.*, 1987) These findings could therefore be seen as additional proof of the existence of the gel layer.

- The PSD measured by NTA had a strong bias towards the largest particles in the sample since the smaller particles have too low scattering intensity to be detected and tracked. The technique was therefore unable to provide reliable information about these samples.

3.2. DETECTION OF HEAVY METAL CONTAINING PARTICLES IN SOILS USING ENVIRONMENTAL SCANNING ELECTRON MICROSCOPY WITH BACKSCATTERED ELECTRON IMAGING

3.2.1. **Characterization of toxicological test samples**

Samples of soil that were spiked with Ag particles for earthworm toxicity tests (OECD 222 Toxicity test) were characterized by ESEM in paper IV. The sizes of the particles were ~80 nm and their concentrations in soil ranged from 1 to 1000 mg/kg. The particles had been purchased as dry powders and then added to the soil as received, or after first dispersing them in water. The samples were characterized both as prepared, and incubated with earthworms for two weeks.

Microscopic characterization revealed that regardless if the NP powder was applied directly or first dispersed in water, the organisms were exposed mostly to large aggregates (Figure 7). Incubation with earthworms seemed not to affect the aggregation state, but resulted in the particles becoming better intermixed with organic matter (Figure 8). An attempt to disperse these particles was made, but even after extensive sonication the dispersion consisted mostly of aggregates rather than primary particles. The results underscore both the need of characterizing the particles in situ in the test soils, and following adequate dispersion protocols to avoid excessive aggregation and thus provide a presumed worst case exposure scenario.

To provide a means for proper sample preparation, a protocol was developed for dispersing aqueous NP dispersion into soil without inducing aggregation. The Au c_p standards in Table 1 were added dropwise (droplet volume 10 µL) to 0.3-0.5 g soil, followed by intense mixing after each droplet. When these procedures were followed, almost all particles found in soil (Figure 9) were solitary primary particles.

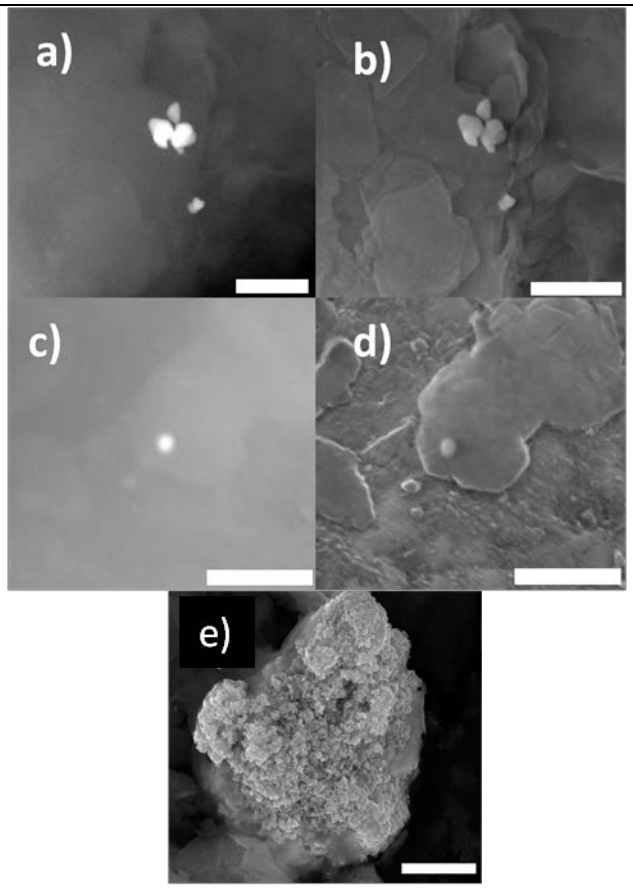

Figure 7 *ESEM images of Ag particles spiked into soil for an OECD 222 toxicity test. BSE, (a) and SE (b) images of a cluster of particles (Scale bars 300 and 400 nm respectively). The individual particles are readily distinguished. c)-d) BSE and SE images of a solitary 80 nm particle (Scale bar 500 nm).e) A large aggregate consisting of a large number of primary particles (Scale bar 2 μm).*

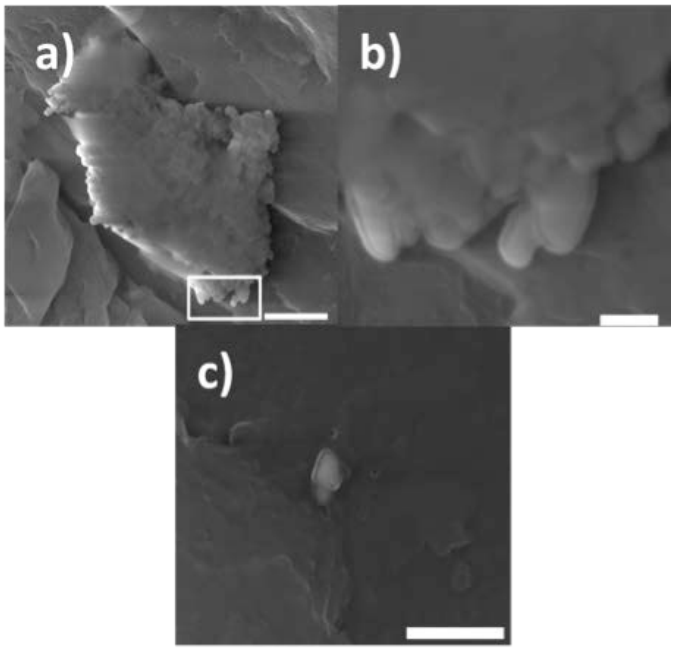

Figure 8 *a) – b) ESEM SE images of an aggregate found in a sample incubated by worms. The area marked in a) is shown at a higher magnification in image b). The core-rim structures consist likely of a ~20 nm layer of organic matter on the particles. A similar structure is seen in image c), which is coming from the same sample. Scale bars a) 500 nm, b) 100 nm, and c) 400 nm.*

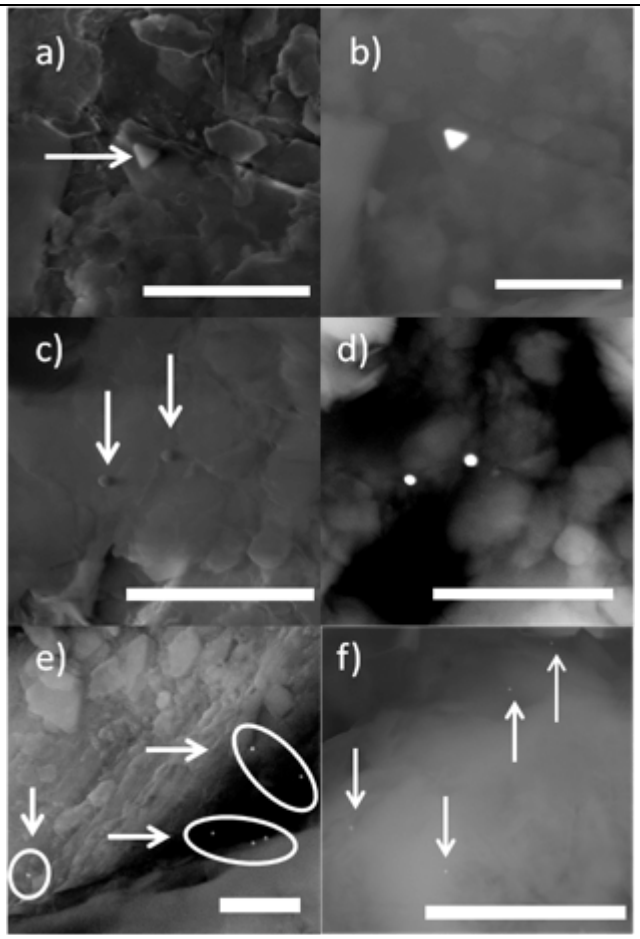

Figure 9 *Au nanoparticles spiked into soil. a) SE, and b) BSE images of a 250 nm particle. c)-d) SE and BSE images of two 100 nm particles. e) BSE image of 50 nm and f) 30 nm particles. The arrows indicate particles. All scale bars are 2 µm.*

3.2.2. **Particle number concentration reference materials**

Because of the lack of suitable absolute measurement methods, there are currently no reference materials with certified number concentration for nanosized particles. Such standard have been created for micron sized particles by measuring the certified c_p using an optical particle counter, and by depositing the particles in a known volume of sample on a solid substrate and counting each of them by light microscopy. (Sakaguchi and Ehara, 2011) Sample preparation and counting of nanosized particles using electron microscopy is not as straightforward because of the propensity of small particles to aggregate during the subsequent drying step, and because the high magnifications that are necessary for visualizing the particles allow only to count a small fraction of them. Optical particle counters are not likely to achieve close to 100 % counting efficiencies for such small particles, because they scatter enough light to be detected only in the part of the laser beam where the illumination is most intense, and the sheath flow cuvettes typically used do not have an accurately defined volume.

In lack of validated direct methods, the c_p of NP dispersions is often calculated from the measured diameter and mass concentrations of the

particles assuming a spherical shape. Particle counting methods such as nanoparticle tracking analysis (NTA), laser induced breakdown detection (LIBD), and electrospray scanning mobility particle sizer (ES-SMPS) are in general calibrated for c_p using such reference dispersions. As long as the particles are truly spherical, the c_p calculated by this analyte mass method becomes as accurate as the uncertainty in diameter and mass concentration permit. The spherical assumption is probably valid for particles such as polymer latexes, and silica sols, but these particles are not suitable for all applications.

Table 2 *Number concentrations obtained using different methods and SEM diameters of the Au dispersions. The uncertainty values are 95% confidence intervals due to variation among replicate experiments. For the total Au concentration methoduncertainty in particle size has also been taken into account.*

Size / Method	Counting particles on filters (Particles mL^{-1})	Total Au concentration (Particles mL^{-1})	Nanoparticle tracking analysis (Particles mL^{-1})
250 nm 423.0±13.6 nm	$9.9*10^7$±6.6.*10^7	$1.3*10^8$±$1.1*10^7$	$4.11*10^8$
100 nm 228.1±16.8	$4.6*10^9$±$2.2*10^9$	$9.9*10^8$±$9.4*10^7$	$8.70*10^9$
50 nm 63.5±2.6	$3.8*10^9$±$3.2*10^9$	$3.2*10^9$±$1.2*10^9$	$4.33*10^9$
30 nm 26.9±0.1[#]	n/a	‡$2.45*10^{11}$ †$2.1*10^{11}$±$2.1*10^{11}$	$2.33*10^{11}$

[#] *Value certified by NIST*

‡ *Value determined using concentration certified by NIST*

† *Value determined using concentration measured here.*

In this work, the development spICP-MS and quantitative BSE imaging required c_p standards based on heavy elements. Metallic NP are in general faceted, and for many samples deviations from the assumed spherical geometry could introduce significant errors. Therefore a feasibility test was conducted of determining c_p of Au NP dispersions by counting them on filters. The NP in a sample having a known volume were deposited on filters with known areas. The surface concentrations (particles m^{-2}) on filters were determined by BSE imaging in SEM (Papers IV, and VI). Knowing the area of the filter that was imaged and where particle were counted allowed calculating the total number of particles that was present in the deposited sample. The experiments were carried out for 50, 100, and 250 nm nominal diameters Au NP. Measuring the Au concentrations in the filtrate with ICP-MS showed that the gold particles were nearly quantitatively retained on the filters.

Secondary electron images of the particles located on filter surfaces are shown in Figure 10, and examples of the BSE images used for counting particles are displayed in Figure 11.

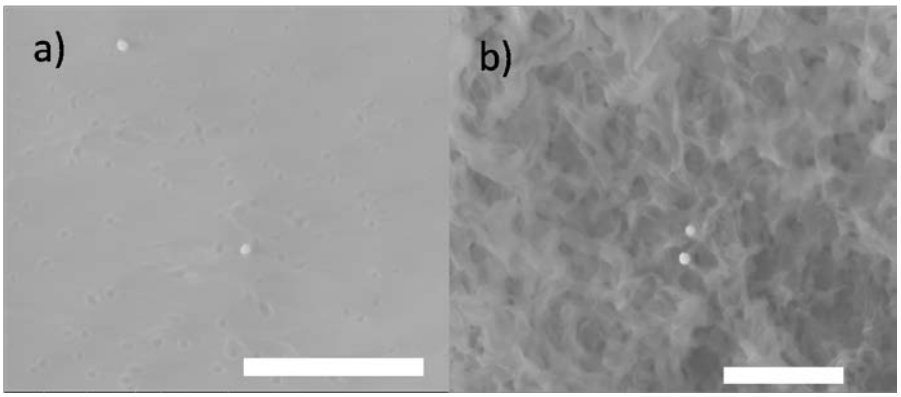

Figure 10 *SE images of AuNP deposited on filters. a) BBI 100 nm nominal diameter AuNP on a 50 nm nominal cut off nuclepore track etched polycarbonate filter. b) BBI 250 nm nominal diameter AuNP on 100 nm nominal cut off cellulose ester membrane. See papers IV and V for details. Scale bar 2 μm.*

The results (Table 2) were in relatively good agreement with the c_p obtained by the total analyte mass method, and NTA. The NTA result seems to slightly overestimate the concentration as explained below. The variation among replicate experiments was large because the particles were not homogenously distributed on the filter surfaces, and the high magnifications (> 3000 times) only allowed examination of a small fraction (~0.001 %) of the total filter area (9.6 cm^2). Some aggregates were also observed. Extensive aggregation during sample preparation would result in an underestimation of the particle number concentration. The precision of the filter deposition method is likely to improve if the particles could be deposited on a small enough area (e.g. < 1 mm^2) so that more particles could be counted. The increased aggregation that might result from forcing the particles into a smaller area could be counterbalanced by diluting the dispersions.

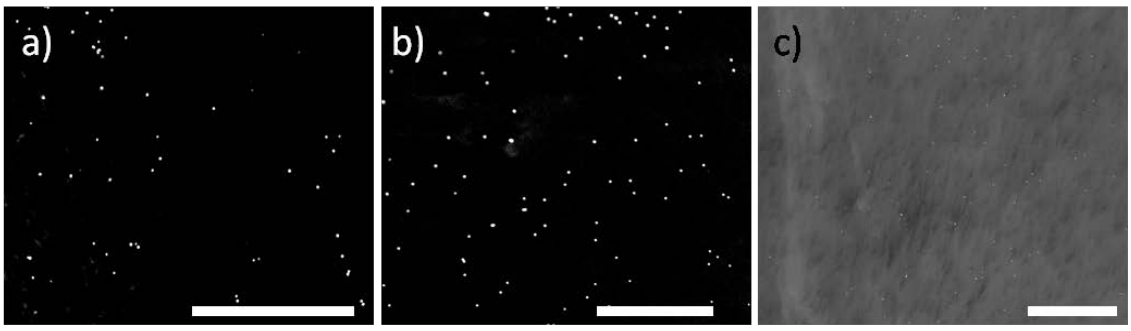

Figure 11 *BSE images of a) 250 nm, b) 100 nm, c) 50 nm nominal diameter BBI AuNP deposited on filters. (Scale bars 20, 10, and 5 μm respectively)*

3.2.3. **Quantitatative ESEM-BSE imaging**

Since a vast range of sample types can be characterized with no, or very little preparation, ESEM forms a suitable base for developing particle quantification methods for solid matrixes (Paper IV). It can be assumed that the number of particles that are visible per imaged area is proportional to their number concentration in the sample. However, to be able to quantify the particles per volume or mass of sample, it is also necessary to know how deep in the matrix particles can be detected, and take into account topographic effects whenever the surface is not flat (Figure 12). The relation between c_p and the number of particles, N counted per in an imaged area, A_i is then given by:

$$N = c_p \chi A_i \qquad (14)$$

where d_s is the sampling depth of the electron beam, and χ is a factor that takes into account topographic effects.

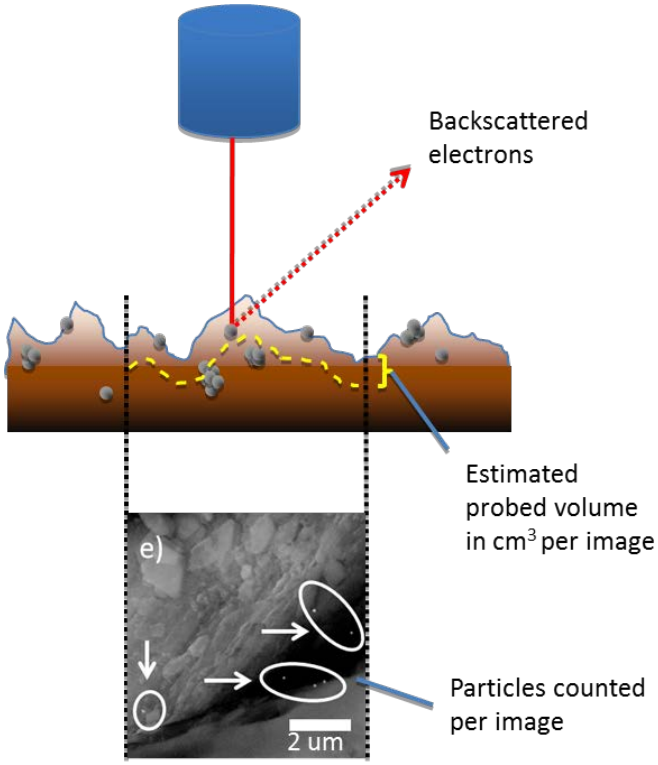

Figure 12 *Schematic showing the principle of quantitative BSE imaging*

An estimate for the d_s was calculated using the Kanaya Okayama, (KO) electron range in combination with an expression giving the fraction of the KO range from which backscattered electrons are emitted. (Kanaya and Okayama, 1972, Goldstein *et al.*, 2003) Because the soil is heterogeneous, the calculations were performed for several soil components and electron beam incidence angles. The concentration of

Ag NP in the toxicological test soils was quantified in Figure 13 using the deepest, (2.6 μm; Organic matter, 0° incidence angle), and shallowest (0.62 μm; SiO_2, 45° incidence angle) calculated sampling depth, and their average. It was assumed for these calculations that the surface is flat.

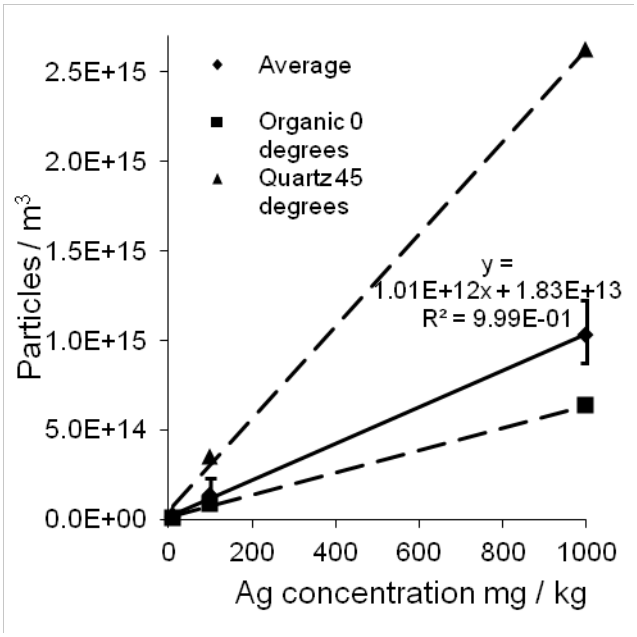

Figure 13 *Particle number concentration as a function of added mass concentration of silver particles in soil. The concentration was calculated for the highest and lowest sampling depths in Table 2 of paper IV and their average. Linear functions were fitted to these data and the fitting parameters are shown for the averaged sampling depth. The error bars correspond to 95 % Poisson confidence intervals for the particle count.*

The number concentration depends linearly on the mass concentration despite of the extensive aggregation. It was however found that the concentrations of the gold nanoparticle c_p standards were overestimated 3-5 times using the KO model. This is partly due to the rough topography. For non-flat samples, the area that is actually examined is larger than the nominally imaged area.. The interior of the large silica grains are not examined by the electron beam either. The particle concentration is thus higher in the volume of soil that is actually examined by the electron beam than in the soil as a whole. Therefore to obtain the most accurate results, an effective sampling depth, S should be determined by spiking dispersions with known c_p into the soil:

$$S = \frac{N}{c_p A_i} \qquad (15)$$

S for the Au NP is shown as a function of their diameter in Figure 14. The sampling depth is size dependent, because larger particles scatter more electrons and can therefore be detected deeper in the soil. Starting from Rau and Reimers model (Rau and Reimer, 2001) for the BSE

contrast produced by a layer of a differing material as a function of its depth in a matrix, the following equation was derived for the S as a function of particle diameter.

$$S = k_p \frac{R_{KO}}{a} ln\left(\frac{V_{part}(\eta_{part} - \eta_{back})}{K_{min} 2\eta_{back}}\right) \quad (16)$$

k_p, and a are constants, V_{part} is the particle volume, K_{min} is the minimum detectable contrast, and the η_{part} and η_{back} are the backscattering coefficients of the particle and background respectively. Here it was assumed the particles were considerably smaller than the interaction volume of the electron beam, and that the contrast produced by particles is proportional to their volume. The S is thus a logarithmic function of particle size. Such function fitted well the experimental data in Figure 14.

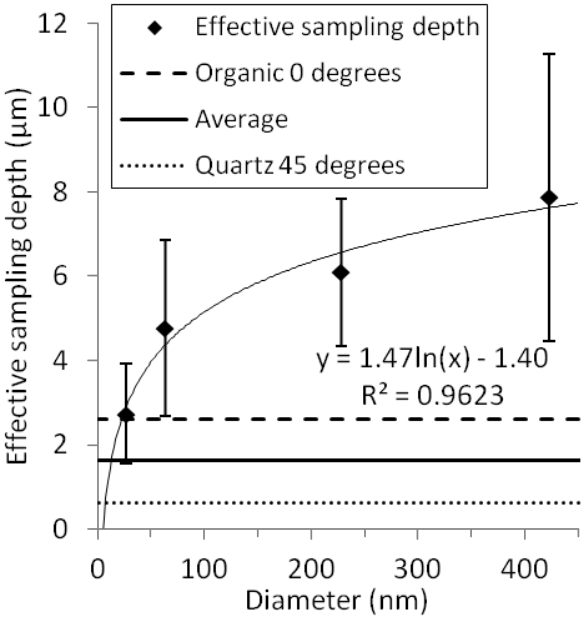

Figure 14. *Effective sampling depth as a function of particle diameter for AuNP spiked into soil. The horizontal lines show the plausible range of sampling depths calculated by the KO model.*

The smallest concentration that is possible to quantify depends on how much time can be invested for finding a statistically significant number of particles. It was estimated that it would be practical to quantify concentrations down to ~10^{12} or 10^{10} particles m^{-3} depending if automated SEM is used or not (Figure 15). Setting a definite size detection limit is also difficult, however, while NIST 30 nm CRM NP (certified SEM diameter 26 nm) could be quantified, the 10 nm CRM (certified SEM diameter 8 nm) were too small for such characterization to be practical.

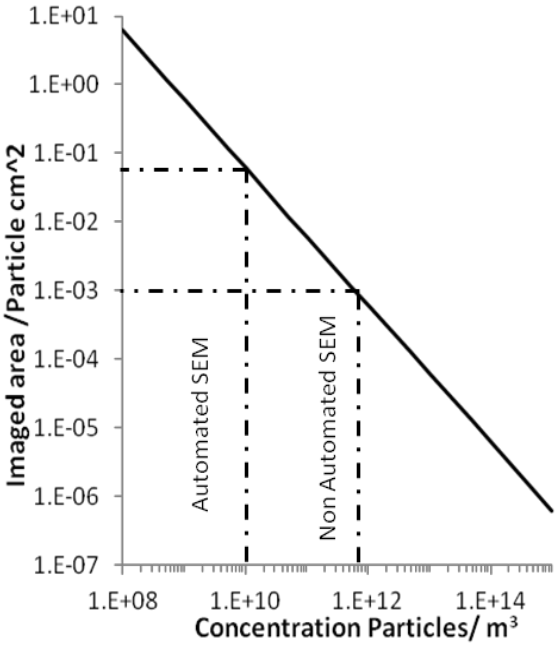

Figure 15. *The area that needs to searched on average to find one particle. The estimated quantification limits for automated and non-automated SEM are indicated as dashed lines. The areas were estimated using the KO model and assuming a flat surface.*

3.3. NANOPARTICLE TRACKING ANALYSIS

3.3.1. **Validation of particle sizing and concentration determination**

Equations describing aggregation and sedimentation rates of NP as a function of their number concentrations and size distributions have been produced for environmental fate modeling.(Arvidsson *et al.*, 2009) For these models to be useful it is required that these parameters have been measured in a large number of aquatic environments. The capabilities of NTA to provide such data was evaluated in paper I.

The image processing parameters (e.g. Gain, Blur, Detection threshold) were optimized to maximize the number of particles identified as such, and tracked. What the most suitable values of these parameters are is of course somewhat subjective, but it was confirmed in paper I that the sizes measured by NTA were according to expectations for polystyrene (> 70 nm), and Au size standards (> 30 nm) for both standard (Marlin), and a high sensitivity (Andor) cameras. The size distributions seem to be broadened since the particles can seldom be tracked long enough to produce statistically accurate estimates of their diffusion coefficients.

The c_p is determined from the average number of particles that are being tracked at a given moment. The concentration response was found to be linear in the range where added NP outnumbered the background contamination, but overlap between light blobs were not so significant (10^6-10^9 particles mL^{-1}) (Figure 16). The intensity of the laser beam decreases with the distance from its center. The more light the particles

scatter, the further from the beam center they can be detected. The inhomogeneous illumination therefore results in an increased volume of detection, and therefore sensitivity, for particles that are larger or consist of materials providing stronger refractive index contrast. Calibration for concentration should therefore preferentially be done using particles with a similar ability to scatter light as the particles of interest. A model for the sensitivity as a function of light scattering power was developed and discussed in papers II, and III. The sensitivity was assumed to be proportional to the detection volume, V_{det} where the intensity of light scattered by the particles exceeds minimum intensity for becoming identified as a particle, the detection threshold, I_{thresh}. The following equation for the V_{det} was derived in paper II.

$$V_{\mathrm{det}} = L\pi c \ln\left(\frac{KA}{I_{thresh}\sqrt{\pi c}}\right) \qquad (17)$$

Here A is a constant proportional to the intensity of the beam, and c is $2*\sigma^2$, with σ being the standard deviation of the presumably Gaussian beam.

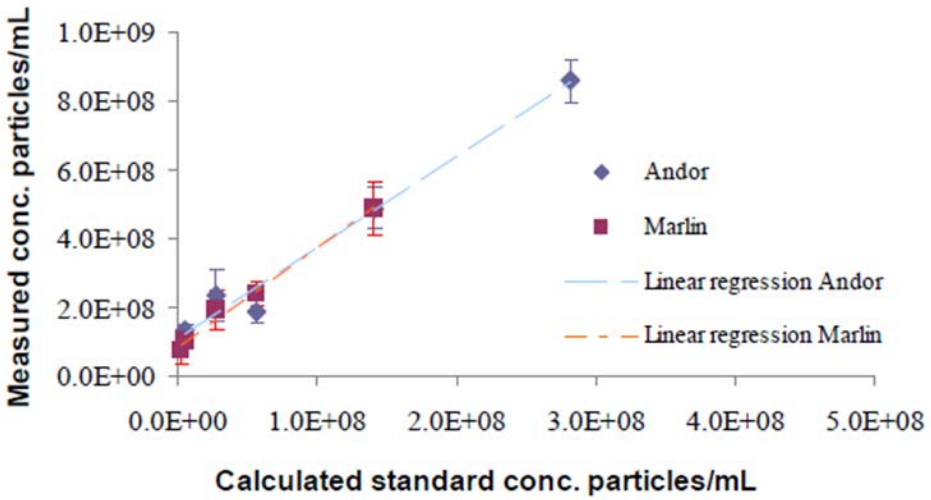

Figure 16 *concentration calibration curves for 60 nm AuNP obtained with standard, (Marlin) and high sensitivity (Andor) cameras.*

Since the actual beam shape is not known, the intensity of scattered light and sensitivity was calculated as a function of particle diameter for polystyrene and gold NP for two assumed values of c in Figure 16. The detection threshold was set thus that the smallest detecTable polystyrene particle size was 30 nm. Note that the model does not take into account that for large particles the V_{det} becomes limited by the dimensions of the imaged area, and the depth of focus of the microscope rather than scattering power of the particles.

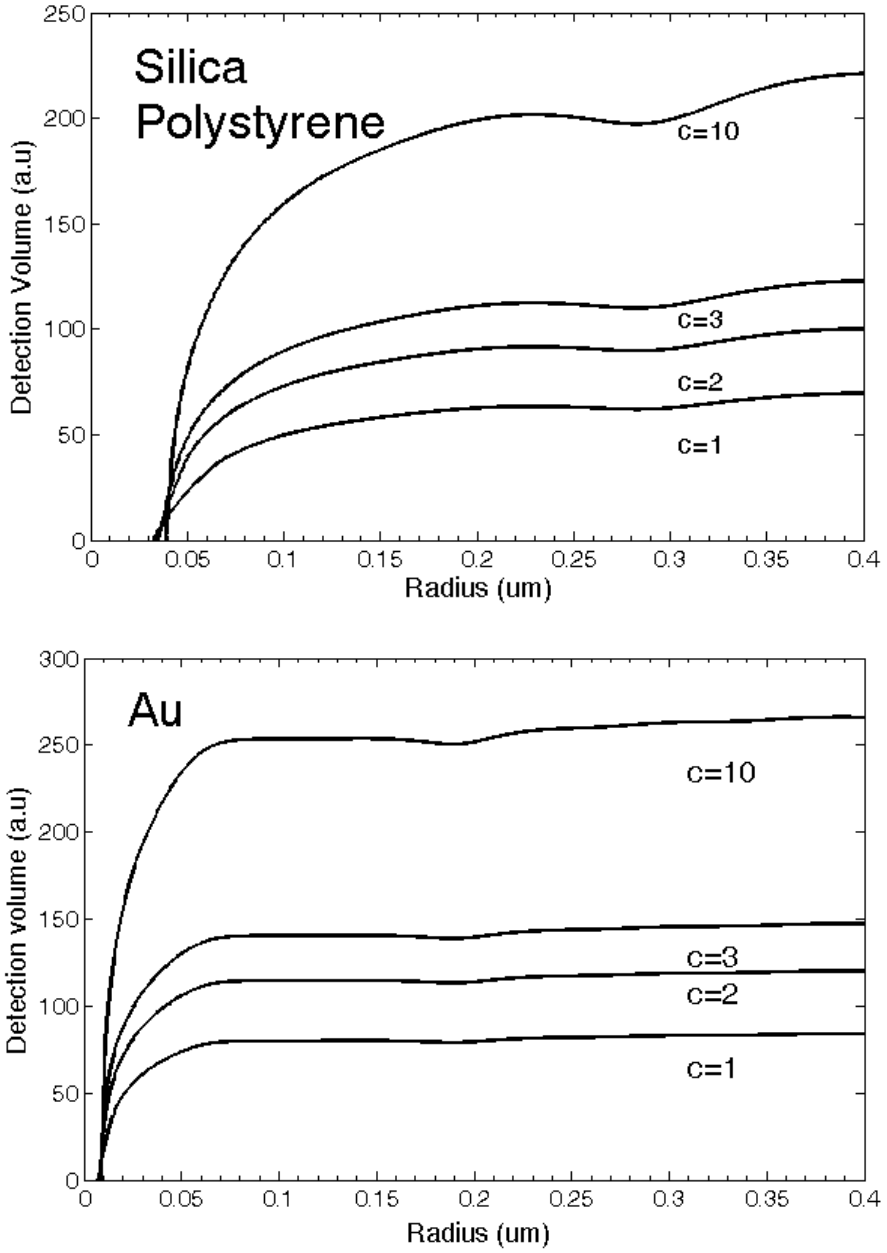

***Figure 17**. The detection volume as a function of size calculated for Au and SiO_2. See paper III for details for such calculations. The refractive index of SiO_2 (1.5) is close to that of polystyrene (1.55-1.6) so the silica data can be used as an good approximation for polystyrene as well. The calculations were repeated for 4 different beam shapes with the parameter c in equation 17 ranging from 1 (sharp beam profile) to 10 (Blunt beam profile). The intensity parameter A and I_{tresh} were the same for all calculations.*

For both gold and polystyrene, the curve of sensitivity as a function of particle size can be divided into two regions (Figure 17). For particles close to the visualization limit, sensitivity increases rapidly with size. For particles considerably larger than the smallest size that can produce a detecTable light spot, the visualization limit, it becomes a rather weak function of size. Particles whose sizes falls into the first region may be visualized; however there will be a strong bias for the larger particles. It was this phenomenon that probably was encountered for the silica

particles. In the second region the size distribution is measured relatively accurately; however the concentration may be over- or underestimated depending if the particles are stronger or weaker light scatters than the calibration standard. The sensitivity depends on the shape of the beam. Sharper beams (small *c*) result in visulisation limits shifted to smaller particle sizes than blunt beams. However, the sensitivity for large particles is higher for more blunt beams (large c), since the light is spread over larger volumes.

3.3.2. **Characterization of environmental samples**

In paper I, c_p and size distributions in water from a large number of aqueous environments in Gothenburg area was measured by NTA. The c_p ranged from ~ 10^8 particles mL^{-1} in coastal seawater to ~10^9-10^{10} particles mL^{-1} in lake and river waters. The c_p in treated Waste water treatment plant (WWTP) effluent was ~10^{10} and that in highway storm water was $1.4*10^{10}$particles mL^{-1}. The concentrations are thus within or close to the dynamic range of the instrument. Furthermore, the c_p determined by NTA correlated with turbidity measurements; especially the samples forced through a 450 nm syringe filter, because these samples were less affected by a few anomalously large strongly scattering particles.

A collection of size distributions of the environmental colloids are shown in paper I. The overall shape of the size distribution was similar for all samples, except for the WWTP effluent. The size distribution was bimodal with a large peak at 100 – 250 nm, and a minor or a shoulder peak at ~50 nm. The particle size distribution in environmental waters has previously been found to follow the Pareto power law (Filella, 2007):

$$\frac{\partial N}{\partial d} = ad^{-b} \qquad (18)$$

Such a distribution arises in systems where there is a constant source of particles that grow by aggregation and are subsequently removed by sedimentation. Equation (18) fitted well the part of the size distributions for diameters larger than the modal value. The possibility exists that the bimodal size distributions observed here arised by aggregation of small particles. However, it is more likely that the observed modes reflect distinct sources of particles. A plausible candidate for the smaller particles is the nearly ubiquitous iron- and aluminium(hydr)oxides, as due to the low scattering power of biopolymers and NOM, the size distribution below 100 nm is likely to reflect mostly that of inorganic particles. The larger mode might be due to clay particles.

The size distribution of the WWTP effluent sample was monomodal, and had a peak around 70 nm. The decrease in concentration for still smaller particles is likely to be caused by a drop in sensitivity. The size distribution of particles in a different sample of treated WWTP effluent was determined by TEM. The size distribution is shown in Figure 17. No chemical or structural information could be obtained for this sample; however, since the organic matter is unlikely to produce enough contrast to be visualized, the particles included in the distribution are probably mostly silicates and metal oxides. The first peak of particles that are a few nanometers in size might be analogous to the nucleation mode for aerosol particles. It is likely to consist of particles that are recently nucleated as a result of redox cycling or precipitation processes. The second peak at around 5-10 nm might be analogous to the accumulation or Aitken mode, where particles grow by Ostwald ripening or aggregation. Aggregation, deposition to larger floccs and eventually sedimentation likely cause the concentration of still larger particles to decrease producing the Pareto distribution.

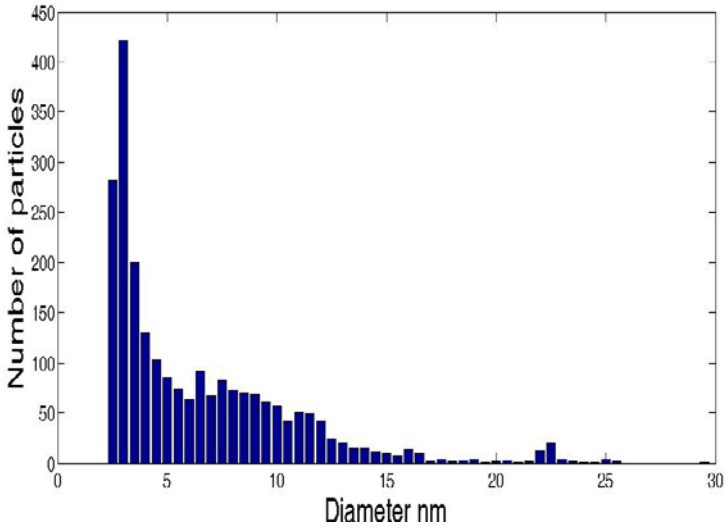

Figure 18. *TEM Size distribution of inorganic NP in WWTP effluent. Note that particles smaller than 2 nm are omitted since they cannot be reliably distinguished from the background.*

NTA is thus concluded to provide accurate number concentrations as long as the optical properties of the calibration standard do not differ markedly from that of the analysed particles. A set of representative values for c_p and number based PSDs for different aqueous environments were obtained which could be useful for environmental fate modeling. In paper II it was demonstrated that it is possible to discriminate strongly scattering Au particles spiked into juice from the predominantly organic background particles based on the scattered light intensity. This could open new venues of research.

3.4. SINGLE PARTICLE ICP-MS

3.4.1. **Determination of nebulization efficiency**

It has been suggested that f_{neb} could be calibrated by counting particles in standard particle suspensions of known c_p, or by adjusting f_{neb} to reproduce the mean diameter of a reference particle suspension. (Pace *et al.*, 2011) However, there are yet no reference materials with certified number concentrations. The diameters of the NIST CRM particles that have been used for such purposes are certified on a method by method basis, with differences amounting to ~ 5 %. None of these is the number weighted volume average that is measured by spICP-MS. In addition, the use of standard nanoparticles increases the cost of analysis. For example, if the f_{neb} would be calibrated using the certified size of NIST gold nanoparticles, a separate calibration is required using dissolved Au standards in addition to the calibration for the element of interest.

Using direct methods for determining the f_{neb} can reduce cost and has potential to achieve higher accuracy. Here, the waste collection method (Browner 1982) was employed for that purpose. Because ions are depleted from the vicinity of solvent surface, the concentration of analyte becomes lower in smaller particles having larger specific surface areas. Since the smaller droplets have a higher propensity to enter the plasma, analyte is redistributed from the plasma to the waste flow. Therefore one can distinguish between a mass-based f_{neb}, and analyte-based f_{neb} that takes into account partitioning effects.

In paper V is shown that using the analyte-based f_{neb} improves the accuracy of calibration for particle mass compared with the mass based f_{neb}. The partitioning effects may not be the same for particles as for dissolved analyte, but it has been found that the ICP-MS signal from NP dispersions is the same regardless if the particles are digested or not. Possible differences in partitioning mechanisms between dissolved analytes or particles are thus probably not qualitatively important, at least in the case of the relatively small particles studied in the present work. Therefore, until particle partitioning has been investigated more closely, the c_p was determined using the analyte-based f_{neb}.

3.4.2. **Accuracy of particle sizing**

Accurate measurement of f_{neb} is challenging, however because any uncertainty in f_{neb} is propagated to the particle diameter as its third root, spICP-MS may be more robust towards error in this parameter compared to other sources of error. Other sources that were investigated were the dead time correction and incomplete particle events. The dead time correction is applied automatically by the instrument when

measuring relatively high analyte concentrations in count mode to account for ions that arrive at the detector while it is still counting the previous ion. During a particle event, the ions arrive at considerable higher frequencies compared to dwells without particle events. Unless corrected for, the dead time error may cause relatively large particles to appear smaller. (Olesik and Gray, 2012) However, knowing the duration of the ion burst, it is possible to calculate the average count rate during the particle event which can then be used for dead time correction (Paper V).

The occurrence of incomplete particle events is to a large extent determined by the dwell time, t_{dwell}. The ratio of particle to background signals increase with shorter t_{dwell} (equation 5), but at the same time, the frequency of particle events which do not fully coincide with the dwell increases. The incompletely measured particle events increase spread in particle signals, and the mean particle diameter becomes biased towards smaller sizes. In addition, with increasing t_{dwell}, the chance of more than one particle arriving in the same time increases as well and the mean particle diameter becomes biased towards larger sizes. The effect of t_{dwell} is illustrated in Figure 19 where frequency-intensity histograms of AgNP of 80 nm nominal diameter are measured with 1, 5, and 10 ms dwell times. At 1 ms t_{dwell} a large fraction of the particle events are only partially measured and accurate sizing becomes impossible.

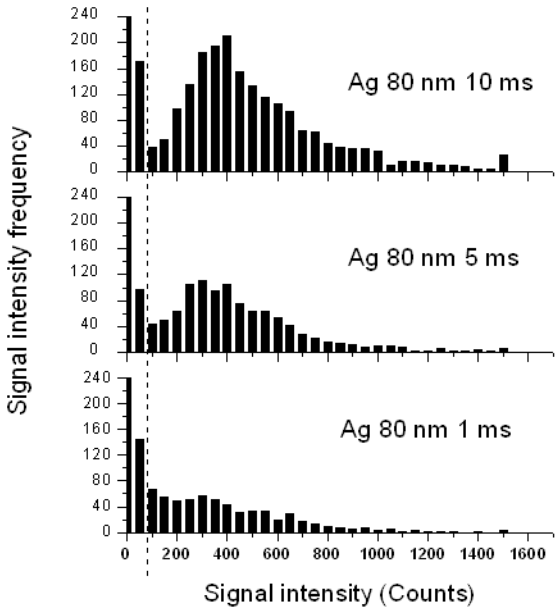

***Figure 19**. Frequency-intensity histograms of 80 nm AgNP measured with dwell times of 1, 5, and 10 ms. The dashed lines indicate the particle detection threshold.*

To judiciously choose t_{dwell}, the fraction of the ions in a particle event that is on average measured, f_d was calculated numerically after

determining the duration of Gaussian ion bursts arriving at the detector. These burst lasted 0.48 ms (Figure 19) and f_d could then be calculated using equation (19) as derived in paper V. Equation (19) assumes that DL_s is 0 or in other words, all particle events occurring at the detector are large enough to be recognized as such:

$$f_d = \frac{t_{dwell}}{t_{dwell} + t_b} \qquad (19)$$

In addition, equation 19 is only valid when $t_{dwell} > t_b$, where t_b is the duration of the ion burst explained in paper V. The f_d calculated using equation (19) at increasing t_{dwell}, agree closely with values calculated numerically. Figure 20 shows that the error introduced by incomplete particle events, reduces as the dwell time is increased, as already suggested by Figure 19. In the case of Figure 20, a dwell time of 5 ms may lead to an acceptable underestimation of f_{d} and thus particle size.

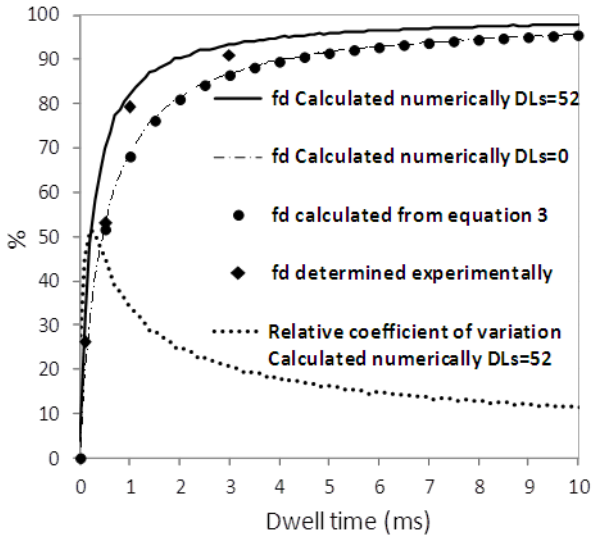

***Figure 20**. The average fraction of ions in the particle events(Ag ~60 nm) with an ion burst duration tb = 0.48 ms that are appearing in each dwell, fd, at different size detection limits, DLs ,are plotted as a function of dwell time for both theoretical and experimental data. The relative coefficient of variation (spread) of particle signal intensities due to incomplete particle events is also included.*

Table 3 *SEM and spICP-MS diameters of nominally 80nm AgNP, and 50 nm AuNP shown together with the magnitudes of bias and uncertainty in the spICP-MS measurements. The spICP-MS diameters were corrected for bias, and the corrected values are given with the 95 % confidence interval due to* Δf_{neb}.

Particles	spICP-MS $d^{\dagger}$	Dead time‡	Incomplete particleevents‡	Δf_{neb}	Corrected spICP-MS d	SEM d
80 nm AgNP	56.24 nm	-0.9 %	-1.2 %	-15.1 % +11.5 %	48.8 - 64.0 nm	62.0 nm
50 nm AuNP	61.06 nm	-3.3 %	-1.2 %	-1.9 % +1.8 %	62.6 - 65.0 nm	63.5 nm

† Measured using the analyte based f_{neb}. *‡ It was assumed that the* t_b *of Au particles equaled that measured for Ag.*

The identified bias and uncertainties in these measurements are listed in Table 3 showing that the nebulization efficiency is not always the largest source of error, but error due to incomplete particle events and dead time correction can be compensated for bias. This is discussed in detail in paper V. In Figure 21, the size distributions measured with spICP-MS are compared with reference distributions measure by SEM using the procedures deemed to be reliable for the silica samples

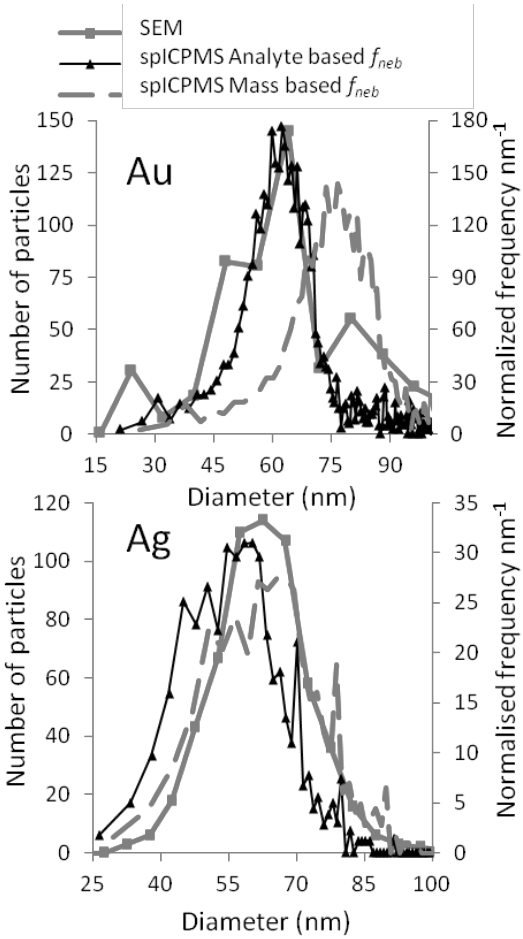

Figure 21 *SEM and spICP-MS size distributions of the 80 nm AgNP and 50 nm AuNP. The spICP-MS size distributions were calculated using both mass and analyte-based* f_{neb}.

3.4.3. **Accuracy of number concentration determination**

The random uncertainty in c_p can be divided into components due to the inaccuracy in f_{neb}, counting statistics, and fluctuations in p_p. Figure 22 shows the width of the 95 % confidence intervals of c_p for a sample of AgNP as a function of N due to random error in f_{neb}, counting statistics (Wilson confidence interval), and their combined effects. The confidence interval of c_p was also calculated by a bootstrap method, which should include fluctuations in particle frequency, if present. The bootstrap confidence interval follows closely that due to counting statistics, which indicates that there were no significant fluctuations in p_p. The random uncertainty in c_p can therefore be estimated from the deviation among replicate measurements of f_{neb} and counting statistics.

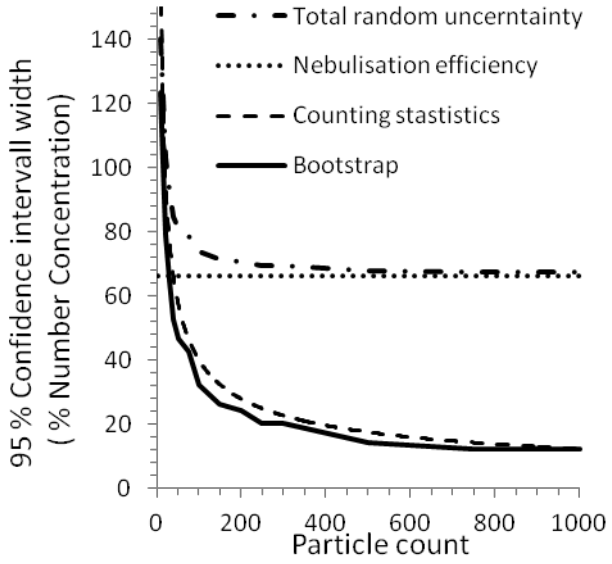

Figure 22 *The width of confidence intervals of c_p is plotted as a function of particle count: The confidence interval of c_p due to total random uncertainty calculated due to both counting stastistics and error in nebulization efficiency (Total random error). The confidence interval of c_p due to the uncertainty in f_{neb} (Nebulisation efficiency). The Wilson confidence interval of c_p due to counting statistics (Counting statistics). The uncertainty calculated using the bootstrap method (Bootstrap).*

In Figure 23, the number concentrations of the three Au dispersions whose c_p were determined by counting the particles on filters were measured using the analyte based f_{neb}, and compared with the reference values in Table 1. The values show reasonable agreement, making it unlikely that there is any systematic bias exceeding few tens of percent in magnitude. This is in agreement with a similar validation study by Laborda *et al.*(2013)

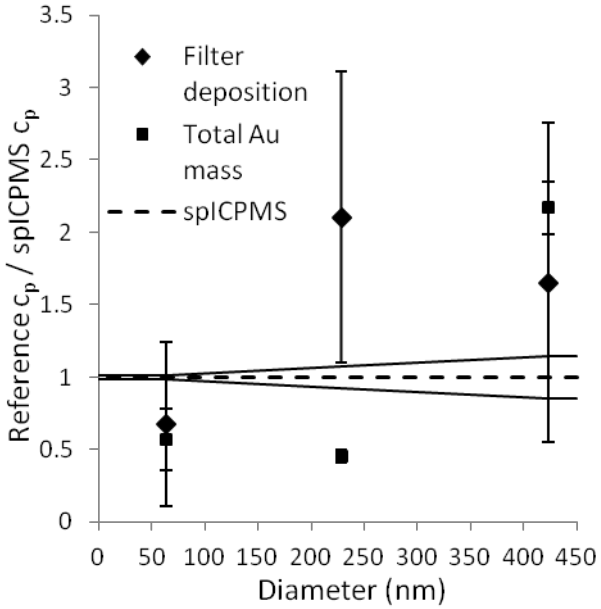

Figure 23. *The ratio of number concentrations measured by the reference methods and spICP-MS. The lines indicating spICP-MS error show the uncertainty due to inaccurate nebulization efficiency, and stochastic error in particle count determined according to equation 7. The uncertainty for the filter counting data is due to variation among replicate experiments, while that of the analyte mass is due to combined effects of uncertainty in particle diameter, and variation among replicate ICP-MS measurements.*

3.4.4. **Noise in particle signals and size resolution**

The capability to resolve particles of different sizes is limited by the noise in particle signals. The magnitudes of different types of noise were evaluated in paper V. The identified noise types were the shot ($\sigma_{IonCount}$) and flicker noise in particle signals ($\sigma_{Proportional}$), noise in the dissolved background signal ($\sigma_{Background}$) that was transferred to the particle signals, and noise due to incomplete particle events ($\sigma_{Incomplete}$). Their magnitudes and the spread due to the polydispersity of the AgNP sample measured in Figure 21 are listed in Table 4. The resolution in particle mass, R_m was defined as three times the standard deviation in I_{part} due to noise. According to this rather strict definition the R_m for these Ag particles is ~ 0.95 fg which corresponds to ~ 12 nm difference in diameter. The noise levels are not higher than that the spread in particle signals, that for most samples will be dominated by the polydispersity.

Table 4. Spread in particle signals due to noise and polydispersity. The listed values are relative standard deviations (RSD).

$\sigma_{Polydispersity}$ †	$\sigma_{Ion\ Count}$	$\sigma_{Proportional}$	$\sigma_{Incomplete}$ ‡	$\sigma_{Background}$	σ_{total}
51 % RSD	4 % RSD	21 %RSD	12 % RSD	1 % RSD	56 % RSD

†Determined from SEM data. ‡ The contribution from incomplete particle events was estimated from Figure 16.

3.4.5. **Trace particle analysis**

The capabilities of spICP-MS for trace particle analysis were investigated in paper VI. Particles can be quantified at orders of magnitude lower mass concentrations than the limit o detection (LOD) of their constituent elements for conventional ICP-MS analysis. Detection of three particle events has been proposed as a LOD for c_p. (Laborda *et al.*, 2013) In principle, the LOD defined this way would be determined by the available sample volume. However, in practice particle contamination builds up, and occasionally outliers in the dissolved background signal are identified erroneously as particle events.

At low particle frequencies or when the particles are close to the size detection limit, the particle events cannot be easily distinguished as a peak or a shoulder in the frequency intensity diagram. Moreover, the frequency of dissolved signal intensities can in general not be fitted accurately enough by simple distribution functions such as the Gaussian or Poisson functions. Therefore one must resort on outlier detection algorithms for discriminating particle events from data points containing background signal only.

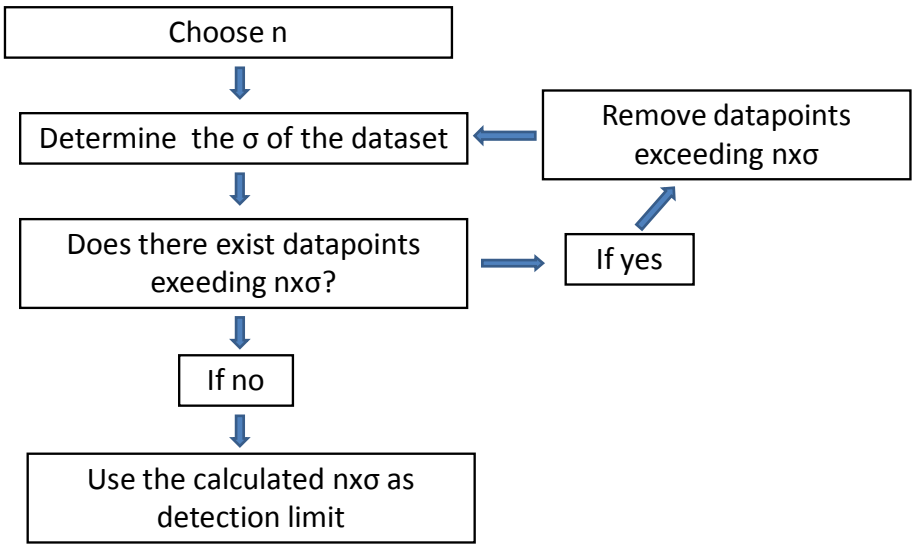

***Figure 24.** Iterative algorithm for particle event detection.*

The algorithm chosen for this work is based on iterative removal of data points whose value exceeds $n*\sigma$, where n is a parameter that is to be chosen, and σ is the sample standard deviation. Data points with $I > n*\sigma$ are removed from the data set, followed by calculation of a new $n*\sigma$ for the reduced data set. The procedure is repeated until no more data points are removed. The removed data points are considered to contain particle events. The course of the algorithm is illustrated in Figure 24.

The parameter n plays a key role as a too low value will result in an unacceptably high frequency of false positives while too high values will result in unnecessarily high DL_s. Figure 25 shows the number of false positives as a function of n in a sample containing dissolved analyte only, together with the particle counts of a sample where the particle signals are well resolved from that of the dissolved background (40 nm Ag), and a sample whose particle signals strongly overlap with the dissolved signal (20 nm Ag). It is necessary to set n to at least 5 to reduce the frequency of false positives to an acceptable level. The particle count for the 40 nm AgNP remains nearly constant for n between 4-12, where the detection limit is put between the set of particle and background signals, while the particle count for 20 nm AgNP is constantly decreasing for the overlapping signal.

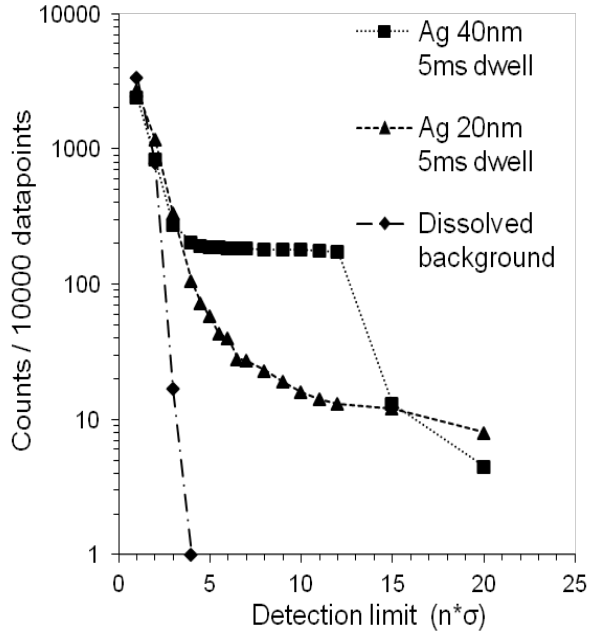

Figure 25 *The number of particle events counted by the iterative algorithm as a function of detection threshold value (n) for data obtained using a 5 ms dwell time. The following datasets are included: 2µgL^{-1} dissolved Ag, and 40nm and 20nm AgNP suspensions.*

Figure 26 shows that particles can be quantified with this algorithm regardless if the particle signals are resolved from the background signals (d_{part}> 40 nm, 5ms t_{dwell}) or not (1 ms t_{dwell}, d_{part}=20 nm). Linear response is obtained for a concentration range of at least two orders

magnitude from where particles from sample dominate over false positives and background contamination (~10^2 particles mL^{-1}), to where the frequency of multiple particle events starts to be significant.

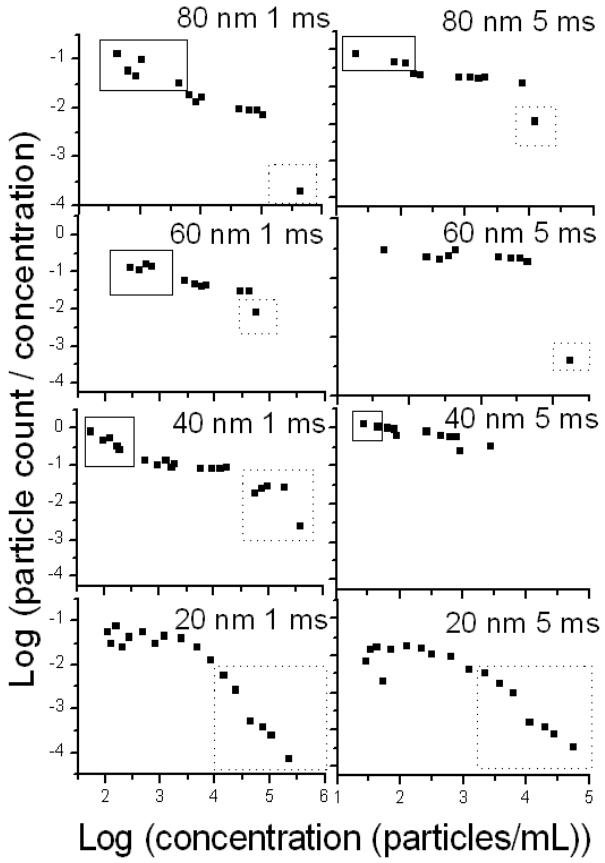

Figure 26. *The logarithm of counted particle events divided by the concentration as a function of the logarithm of concentration. The data obtained for 20, 40, 60, and 80 nm Ag particles using 1 ms (left) and 5 ms (right) dwell time and 5*σ detection threshold is shown. 10 000 dwells were used for each sample. The boxes indicate the region where the relative frequency of false positives, (solid line), and multiple particle events (dashed line) becomes significant.*

For low particle concentrations, where a large fraction of the detected particle events are due to contamination or false positives, equation (20) could be used for calculating the number concentration.

$$C_p = \Delta p_p f_{neb} q t_{dwell} \qquad (20)$$

Δp_p is the difference in frequency of particle events between the sample and the blank. A confidence interval I_C for Δp_p between p_{p1} and p_{p2} can be calculated using:

$$I_c = 2z\sqrt{\left(\frac{p_{p1}(1-p_{p1})}{D_1}\right)^2 + \left(\frac{p_{p2}(1-p_{p2})}{2}\right)^2} \qquad \Delta p_p = \Delta p_p \pm 1/2 \qquad (21)$$

D is the number of dwells acquired and z is the z score of the normal distribution that assumes the value of 1.96 for a 95% confidence interval. A detection limit in the presence of background particle events could thus be defined as a particle frequency for which zero is not included within the confidence interval given by equation 21.

3.5. APPLICATIONS OF SPICP-MS FOR ENVIRONMENTAL SAMPLES

3.5.1. **Nanowash**

The first application of spICP-MS to an environmental sample was presented in paper VII where the effluent of an AgNP producing washing machine (Nanowash) was characterized. In this early work no calibration of signal intensities for particle mass was performed, but by comparing with the intensities of standard NP it could be concluded that these particles were mostly 20 nm or less in diameter. The total particle concentration measured by NTA was considerably higher than the concentration of Ag containing particles, which emphasized the need of developing more selective methods. TEM was used to confirm that the silver containing particles were metallic Ag

3.5.2. **WWTP effluent**

In paper VI The usefulness of spICP-MS as a screening tool for NP was tested on a sample of treated waste water effluent. The sample from the GRYAAB WWTP was taken and analysed already in May 2009, and gives therefore an idea about the NP concentration levels at the beginning of the rapid increase in commercial NP use. To minimize DL_s, the dwell time was set to 0.1 ms. Because the difference between set and effective dwell time would be large (See paper V), the c_p was determined from calibration curves made with 60 nm NIST CRM nanoparticles (the c_p for the standards had been determined using the total analyte mass method). The concentrations were thus more reliable than in another early study of particles in WWTP effluent where the f_{neb} was simply assumed to be 10 %. (Mitrano *et al.*, 2012) Following filtration (a 5 µm prefilter followed by a 450 nm syringe filter), the sample was screened for particles of a range of elements (Ag, Ce, Ti, Si, Zn, Cr, Cu, Mo, Pt, Sb, W, Y, and Zr). Particles consisting of Ag ,Ce, and Ti were found (Figure 27). The concentrations were 9568 particles mL^{-1} for Ag, 2312 particles mL^{-1} for Ce, and 32656 particles mL^{-1} for Ti.

The concentration of Ag particles agreed with what was predicted that time by modeling. However, recent investigations suggest that both dissolved and particulate silver are reprecipitated in WWTP as nanoscale silver sulfide (Ag_2S) particles,(Choi *et al.*, 2008, Kim *et al.*,

2010, Kaegi *et al.*, 2011) in which case it cannot be distinguished whether the Ag in the detected particles was originally released in particulate form or not. The Ag concentrations at GRYAAB have been decreasing since silver halide based photographic film fell out of use. (Praetorius *et al.*, 2013) However, the levels have been increasing again in recent years presumably due to the extensive use of AgNP as antiseptic. Particles of TiO_2 are used in large amounts in *e.g.* cosmetics, sunscreens, and paints. CeO_2 NP are possibly emitted from automobile catalysts and are often used as a marker for traffic related pollution. However, geological sources for the Ce and Ti containing particles cannot be excluded. Titanium minerals such as rutile, brookite and ilmenite are widely spread, and are likely to at least partly contribute to the detected particles. This will be discussed further below.

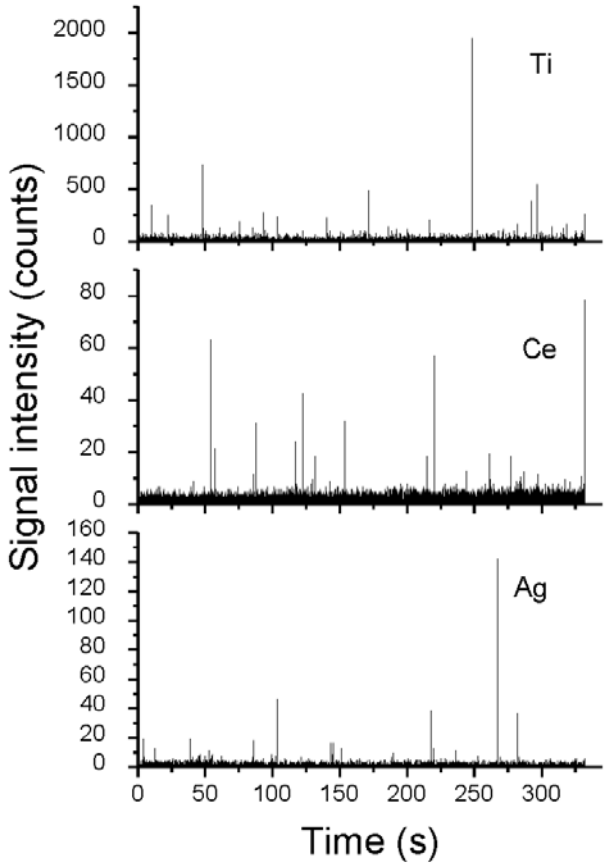

Figure 27. *Time resolved signals of spICP-MS for waste water effluent samples. The monitored elements were Ti, Ce, and Ag.*

Samples of treated WWTP effluent from a pilot WWTP plant where the influent had been spiked with ~ 40 nm AgNP was characterized with spICP-MS (filtration as for the GRYAAB samples, 5 ms t_{dwell}). The size distribution (Figure 28) was in large extent overlapping with the dissolved background, and only the tail of relatively large particles (20-25 nm) could be distinguished. The original particles had been removed by sedimentation or by dissolution.

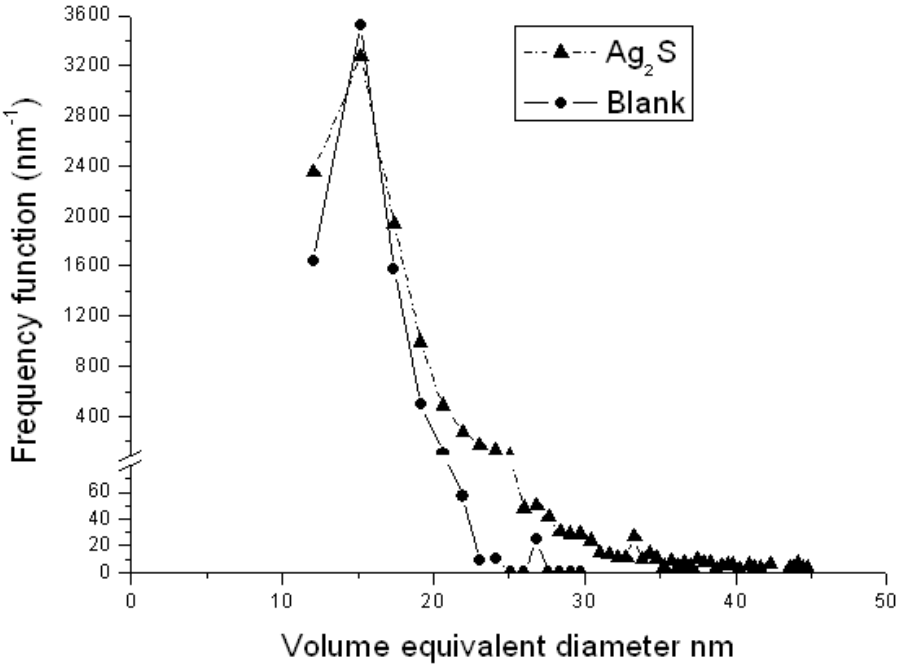

***Figure 28**.spICP-MS size distributions of Ag_2S particles in the WWTP effluent and a blank sample.*

3.6. CHARACTERIZATION OF PARTICLES IN ROAD RUNNOFF USING ELECTRON MICROSCOPY AND SPICP-MS

To make a brief survey of the traffic related particle contamination, a sample of dust was taken from the walls of a highway tunnel (Tingstadstunneln, Göteborg). The most common type of heavy metal containing particle was Fe oxides originating from steel. They were of varying shapes with sizes ranging from few tens of nanometers to tens of micrometers, and contained often significant amounts of alloying elements such as Cr and Ni (Figure 29). The particles found could either originate from top-down fragmentation from road surface and vehicles, but also from bottom-up reprecipitation from dissolved chemical constituents. Another type of contamination was minerals that were most likely ripped from the road surface. Although the particulates dominated by alumina silicates, there are also other compositions. These included zircon and some unknown rare earth minerals (Figure 29). Also large quantities of tungsten containing particles were found. EDX mapping showed that the W correlated neither with Fe or Ca ruling out W minerals such as wolframite and scheelite as the source of these particles.

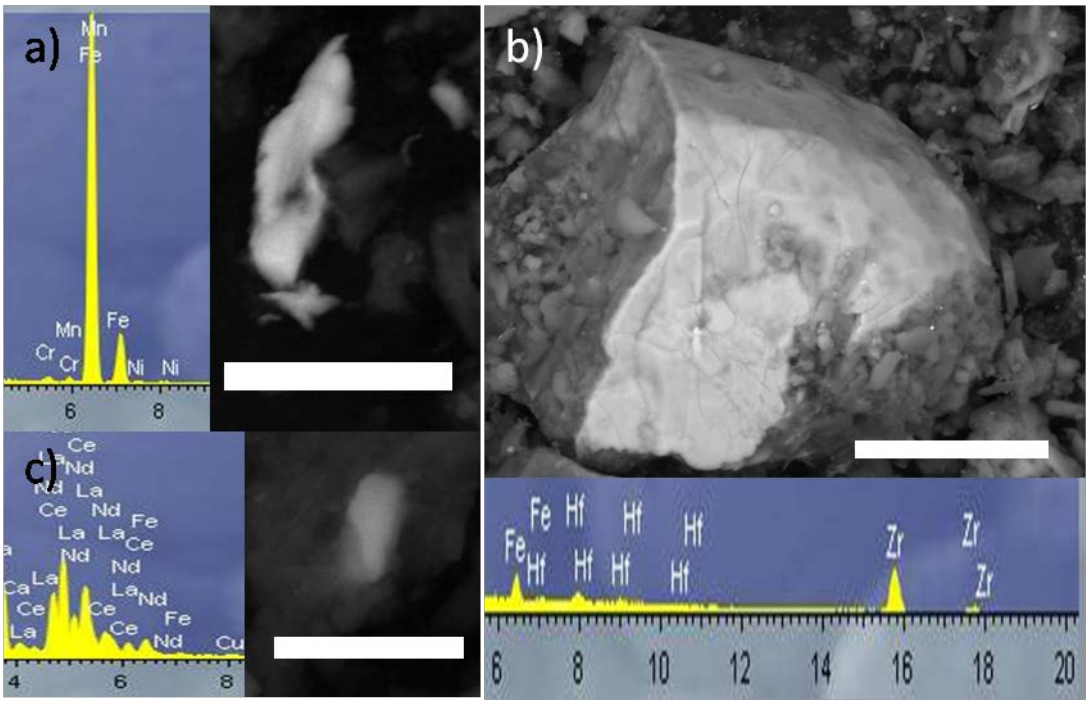

***Figure 29**. Environmental scanning electron microscope BSE images and the corresponding EDX spectra of a) Steel, b) Zircon, and c) rare earth element composed particles found in highway dust. The scale bars are 10, 50, and 10 µm respectively. The energy scale in the EDX spectra is in keV.*

These particles are most likely tungsten carbide originating from winter tire studs and hard coatings (Paper VIII). That tungsten containing particles (of larger sizes) are included in traffic emissions has already been noted in some earlier studies, but relatively high abundances of WC nanoparticles were qualified and characterized in this work. The WC particles were irregular in shape and the sizes of the detected particles span over a wide range from few tens of nanometers to several microns. Figure 30 shows EDX maps and a BSE image of a particle of WC-Co alloy that was probably torn from a tire stud that hit a hard zircon grain on the road surface. In Figure 30 a TEM image of a particle that could be WC, is displayed together with its EDX spectrum and SAD pattern. This particle was found in road runoff water sampled close to the tunnel.

WC particles were measured by spICP-MS in road runoff water collected from a freeway in Gårda in central Gothenburg. The sample was allowed to sediment 3 days at 4 °C, after which it was decanted and filtered with a mesh (> 0.1 mm). The larger particles were removed using syringe filtration with 5 µm, followed by 450 nm nominal cut-off polycarbonate filters. The WC particles in the sample thus represent a long term stable fraction with potential to be transported far.

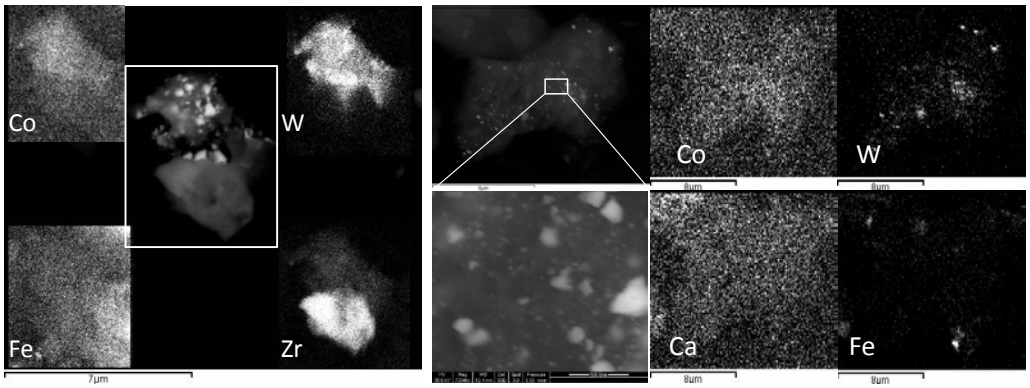

***Figure 30**. Environmental (variable pressure) Scanning Electron Microscopy analysis of road side dust collected at the highway tunnel wall, close to the stormwater collection point. Left: BSE image and Co, W, Fe, and Zr elemental maps of a cluster of Co containing WC particles on a zirconia grain. The scale bar is 7 µm. Right: Low and high magnification BSE images of a cluster of Co containing WC particles. The scale bars are 8 µm, and 500 nm respectively. The area shown in the Co, W, Ca, and Fe elemental maps is that shown in the low magnification BSE image. The scale bar in the elemental maps is 8 µm.*

The sample was measured using spICP-MS with $5*\sigma$ detection threshold and 20 ms dwell time. To obtain the number of W ions coming from each particle, the mean background signal was subtracted from the particle signals. The detection threshold corresponded to a spherical WC particle of 62.5 nm in size. The particle signals were converted to volume equivalent spherical diameters whose distribution is shown in Figure 32. The dissolved W concentration that was determined from the data points that contained no particles was 35.15 ppb. The number concentration of particles with sizes exceeding this value was 46.58 particles mL^{-1}. The fraction of particle-bound W was ~0.44 %, a value that was as calculated by summing the particle signals.

These results can be compared with the study Stolpe *et. al.*(2005). In their work (sampling in February 2004), the total W concentration in a relatively pristine creek located only a few kilometres from the Gårda site was determined to be 0.081 ppb. For this sample, the concentration in the fraction passing 0.45µm filter was 0.0155 ppb while the colloidal fraction 1-50 nm as determined by Flow field flow fractionation coupled to ICP-MS was found to be 0.0019 ppb. Most of the W was thus bound on relatively large particles. The total concentration is close to the global mean riverine W concentration of 0.03 pbb. Considering the different concentrations between the two sites, it becomes clear that significant amounts of anthropogenic tungsten are released into the urban environment. Most of this appears as dissolved in spICP-MS, and it is therefore not likely that total W concentration that pass the 450 nm filter can be used as a proxy for the WC particles.

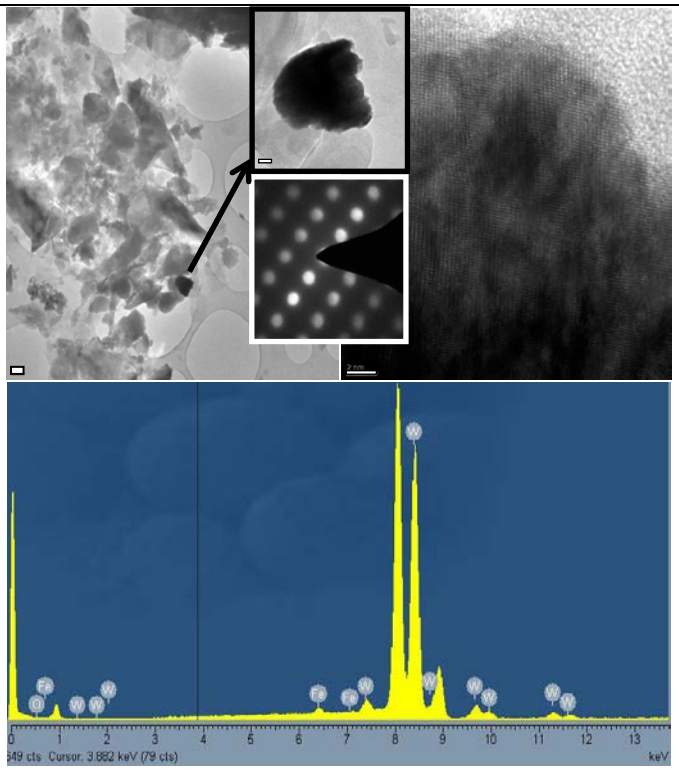

***Figure 31**. Transmission electron microscopy analysis of a WC particle collected at a stormwater collection point near the highway tunnel. The upper left panel shows a complex mixture of particles of different origins and an electron dense (dark contrast) particle that the EDX analysis determined to be composed of tungsten. The upper inserted panel with higher magnification allow estimation of the particle size to approximately 100 nm. The lower inserted panel shows the Selected Area Electron Diffraction image, and a high resolution TEM image of part of the particle, which also allowed a FFT analysis of the crystal structure.*

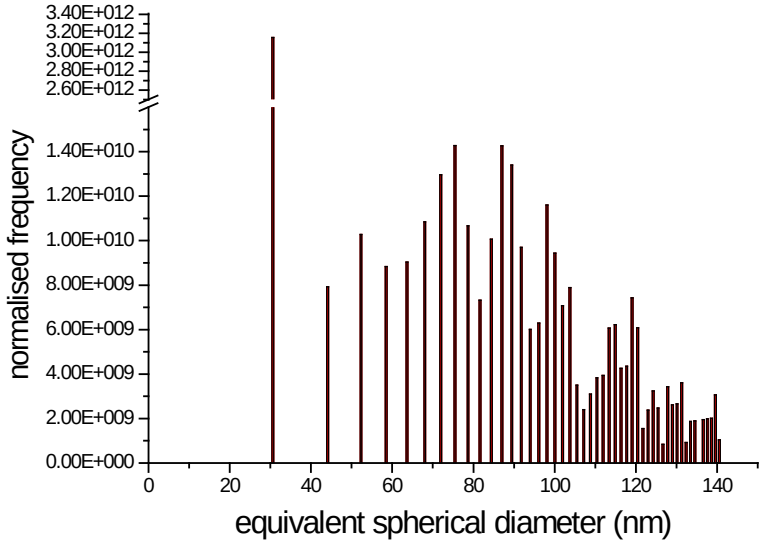

***Figure 32.**spICP-MS size distribution of W containing particles. The rawdata signal histogram is included in the supplementing information together with experimental details. It can be seen that in addition to the nanoparticles there is also an extensive abundance of dissolved ionic tungsten and solids that is originating from particle sizes that are smaller than the detection limit (here set at 5*σ of the background signal).*

4. CONCLUSIONS AND FUTURE WORK

It is concluded that in order to support nanosafety research and regulation, reliable methods for sampling, sample preparation, analysis and validations are urgently need. Furthermore, tools such as certified reference materials and standard methods for absolute particle concentration measurements in the nanoscale domains is crucial for developing particle counting methods. Steps towards creating such standard were made by counting Au particles deposited on filters by ESEM. The approach was considered feasible, however it was also concluded that in order to eliminate error arising from failing to count all particles in the sample, the particles must be deposited on areas less than 1 mm^2. This would require the construction of new filtration devices. The Au standards characterized this way were used to develop particle quantification methods in soil and to validate spICP-MS.

NTA is a minimum-perturbing, rapid, easy, and well suited for providing number concentrations and size distributions that are required for ecotox studies It was concluded that NTA is also capable of providing the overall particle number concentrations, and size distributions in environmental waters that are required to support modeling efforts. However, because the size distributions are skewed towards larger particles for sizes close to the visualization limit; the range of diameters where the technique is reliable must be determined on a material to material basis.

For toxicological tests involving soil biota, *in situ* characterization can be performed by ESEM using the heavy element, high contrast BSE mode. Both the aggregation state and number concentrations can be determined by counting the particles in the obtained images. Without automated instruments ESEM characterization is in most cases limited to relatively high concentrations. Methods based on automated instruments should be developed for quantification of trace level particle contamination in sediments, sewage sludge, and road dusts.

During the intermethod comparison study of particle sizing methods for SiO_2 dispersion, it was found that the commonly used drop cast method for preparing TEM grids gave bias towards smaller particle sizes. The occurrence of sample preparation artifacts is probably not so surprising, but very little work has been done on validating sample preparation methods for reliability. The sample preparation method used for SEM was considered reliable, because all particles in the

analyzed volume of dispersion are retained on the sample holder, and because the results are in close agreement with ES-SMPS.

Another interesting finding is that the hydrodynamic diameter of SiO_2 NP was smaller than the physical diameter measured in dry state. The explanation that lies closest at hand was that a gel layer of silica chains protruding from the surface forms in aqueous environment. The case for silica illustrates how the differences in diameter due to the contrasting environments and physical properties measured by the techniques can be larger than their uncertainty levels.

Due to its reliability and capacity to measure particles on filters, the SEM method was used as a reference method for validating the accuracy of spICP-MS. It was concluded that, provided that the nebulization efficiency was measured, taking into account analyte partitioning between flows towards plasma and waste, the sizes were comparable to those provided by SEM. The smallest detecTable particle size is determined by the magnitudes of noise in the dissolved background signal. For Ag it is close to 20 nm.

The accuracy in number concentration is mainly limited by uncertainty in nebulization efficiency and counting statistics. Comparison of number concentrations determined by counting particles on filters lead to conclusion that spICP-MS is unlikely to be associated with a systematic bias of more than a few tens of percent.

spICP-MS was successfully applied on a range of environmental samples and the quantification of tungsten containing particles at concentrations of a 10^2 to 10^5 particles/mL, or ~100-200 ppt particle bound W demonstrates its capability for monitoring anthropogenic nanoparticles.

spICP-MS as it was performed in this work is not capable of measuring more than one element at a time. Furthermore the size detection limits are insufficient for quantifying *e.g* the small (<20 nm) Ag_2S that are likely to precipitate in the environment.

Time off flight instruments could allow measuring more than one element at a time. (Schilling *et al.*, 2007, Borovinskaya *et al.*, 2013) The detection limit could be reduced by decreasing the noise in dissolved analyte by e.g monodisperse droplet introduction (Gschwind *et al.*, 2011)or by using fast data acquisition with high time resolution as demonstrated in paper V. Powerful tools could be created by coupling spICP-MS to size separation techniques such as HDC, FFF, and SMPS. Pergantis and Heithmar (Pergantis *et al.*, 2012) demonstrated that 2 dimensional size information could be obtained by coupling with HDC, and in this thesis it was shown that size detection limits could be improved by hyphenation with flow-FFF because dissolved analyte is

removed during the fractionation step, and shorter dwell times than what would be feasible in standalone spICP-MS could be used. Steps towards coupling spICP-MS with SMPS has also been taken. (Kapellios and Pergantis, 2012)

spICP-MS and quantitative ESEM imaging are powerful tools for samples on which these techniques can be applied with little preparation. Yet, there are large sample classes which are not amenable for analysis by neither of them. Developing slurry nebulization methods for spICP-MS could enable characterization of dispersions with high content of solids, such as waste water without omitting the larger particles and encountering the risk of introducing artifacts by filtration. Samples such as foodstuffs, biological tissues and waste water sludge would however require digestion prior introduction to an ICP-MS instrument. Since a large fraction of such samples is water that will evaporate in the sample chamber; straight forward characterization without introducing large sample preparation artifacts is not possible by ESEM either. Enzymatic digestion might be able to decompose many types of matrixes without affecting the particles (Beltrami *et al.*, 2011) Samples could also be *e.g.* freeze dried and grinded to provide more suitable matrixes for ESEM (Dudkiewicz *et al.*, 2011) Since particle dispersions are dynamic non equilibrium structures proper sample handling and storage are imperative for the quality of analysis even for the simplest of samples.

One can question if the release of engineered nanoparticles will ever be significant in comparison with the relatively high concentrations of natural nanomaterials that prevail in aqueous environments or the significant amounts of particles produced accidentally due to *e.g.* wear or combustion.

Another question is whether the engineered nanomaterials will turn out to be more toxic or convey other harmful effects that distinguish them from the diverse flora of particles that has surrounded mankind since ages?

Answering these questions requires toolboxes of validated, sensitive, and specific methods that currently exist only for organic and biological molecules. The development of analytical science for nanoparticles is only in the beginning and therefore the knowledge of occurrence, reactions, and toxicity of trace level particles is still very limited and fragmentary.

5. SUMMARY OF PAPERS

The fate of nanomaterials in environmental waters is governed by aggregation and subsequent sedimentation of the large aggregates. Equations have been produced to account for this in environmental material flow modeling. These models require knowledge of number based concentrations, and size distributions including all particle types present in the media. The capabilities of NTA to perform such measurements are evaluated in **paper I**. Number concentrations and size distributions are presented for a number of contrasting aqueous environments in the Gothenburg area.

In **paper II,** the previous work on NTA is reviewed and a critical discussion is provided of its possibilities and limitations. An attempt to model the bias towards large particle sizes that arise due to the inhomogeneous illumination provided by laser beam is presented. The feasibility of using the intensity of scattered light to distinguish strongly scattering Ag particles in food samples are demonstrated, and a discussion is provided about the user defined image processing parameters of the particle tracking software.

An evaluation of the applicability of common PSD techniques (NTA, TEM, SEM, Electrospray scanning mobility particle sizer (ES-SMPS), Dynamic light scattering (DLS), and sedimentation FFF (SedFFF) hyphenated with DLS) for measuring NP of colloidal silica (~35 nm diameter) was carried out in **paper III**. The study aimed to quantify and discuss sources of bias and material specific effects for sizing one of the most produce NP type.

Paper IV addresses three current problems in environmental nanoscience. The first is the lack of characterization and appropriate dispersion methods for nanoparticles in soil for toxicity tests involving earthworms. The capabilities of ESEM for imaging Ag particles dispersed in soil was evaluated and protocol for amending the soil with Au particles without inducing aggregation was developed.

To be able to accurately dose particles, methods for determining c_p in dispersion were evaluated for Au particles (~30 - 450 nm diameter). These included counting particles deposited on filters with SEM, calculating it from the analyte mass, and NTA calibrated using the manufacturer recommended procedure.

The created number concentration standards where used for developing a method for quantifying particles in soil based on counting

them in ESEM images. Different ways of calculating the c_p in soil from the number of particles visible in the images was discussed.

In **paper V,** the c_p standards from previous article and Ag NP are used for evaluation of the accuracy of PSD and c_p measured by spICP-MS. Different sources of bias and the role of counting statistics for the accuracy are discussed.

The capabilities of spICP-MS for characterization of trace level particle concentrations in environmental samples are evaluated in **paper VI**. The work focused on evaluating an outlier detection algorithm for distinguishing the particle events, evaluating the smallest detecTable particle size, and smallest quantifiable concentration. The applicability of spICP-MS as a screening tool for particles in treated Waste water treatment plant (WWTP) effluent was evaluated.

In **paper VII,** spICP-MS is applied for characterizing the effluent of an Ag NP producing washing machine. Although the method was at a poorly developed stage in this work, it is probably the first publication where spICP-MS was applied on a real world sample. In **paper VIII** tungsten carbide particles emitted predominantly from winter tire studs were characterized using combined analytical techniques including both stand alone and spICP-MS hyphenated with flow FFF, SEM on particles found in a road dust sample, and TEM on a particle found in road runoff water. These particles might be associated with special hazards as indicated in occupational toxicology of these materials, and may also imply risk due to their likely persistence in the environment. The need for quantification and suitable methods are discussed.

Data that was not shown in any of the papers on particles detected in road dust using ESEM, and in treated WWTP effluent measured using spICP-MS is discussed in the section summarizing this work.

6. ACKNOWLEDGEMENTS

I would first like to thank my supervisors **Martin Hassellöv**, **Stefan Gustafsson**, and **Geert Cornelis** who made everything possible, by among other things, spending their evenings editing this thesis. I also thank my examiner **Elisabeth Ahlberg** for always seeming to believe in me.

I appreciate the past and present people of the environmental nanochemistry group **Caroline Jonsson, Kajsa Baumann, Julian Gallego-Urrea, Jenny Perez-Holmberg, Karin Danielsson,** and **Tobias Pallander** a lot. I especially enjoyed those summer weeks working with the NTA paper with you Julian and Tobias.

I would also like to thank **Ann-Cathrin Johnsson** for putting me on the right track with the silica paper and **Zareen Abbas** for taking his time to comment the manuscript.

I would like to acknowledge **Kerstin Bohman, Anders Kvist, Alpo Karppinen,** and **Esa Väänänen** for their efforts for making the practical issues work smoothly during my stay here.

Not to forget all the other friendly people at the chemistry department.

I would finally like to thank my family, and especially you **Gulnara** for being the light that lit my path these years.

7. REFERENCES

ALLABASHI, R., W. STACH, A. DE LA ESCOSURA-MUNIZ, L. LISTE-CALLEJA AND A. MERKOCI (2009). "ICP-MS: A POWERFUL TECHNIQUE FOR QUANTITATIVE DETERMINATION OF GOLD NANOPARTICLES WITHOUT PREVIOUS DISSOLVING." JOURNAL OF NANOPARTICLE RESEARCH **11**(8): 2003-2011.

ARVIDSSON, R., S. MOLANDER, B. A. SANDÉN AND M. HASSELLÖV (2009). "MODELING THE EFFECT OF AGGREGATION AND SEDIMENTATION ON PREDICTED ENVIRONMENTAL CONCENTRATIONS OF TITANIUM DIOXIDE NANOPARTICLES." ENVIRONMENTAL SCIENCE & TECHNOLOGY **TO BE SUBMITTED**.

BAALOUSHA, M., Y. JU-NAM, P. A. COLE, B. GAISER, T. F. FERNANDES, J. A. HRILJAC, M. A. JEPSON, V. STONE, C. R. TYLER AND J. R. LEAD (2012). "CHARACTERIZATION OF CERIUM OXIDE NANOPARTICLES-PART 1: SIZE MEASUREMENTS." ENVIRONMENTAL TOXICOLOGY AND CHEMISTRY **31**(5): 983-993.

BATTIN, T. J., F. V. D. KAMMER, A. WEILHARTNER, S. OTTOFUELLING AND T. HOFMANN (2009). "NANOSTRUCTURED TIO2: TRANSPORT BEHAVIOR AND EFFECTS ON AQUATIC MICROBIAL COMMUNITIES UNDER ENVIRONMENTAL CONDITIONS." ENVIRONMENTAL SCIENCE & TECHNOLOGY **43**(21): 8098-8104.

BELTRAMI, D., D. CALESTANI, M. MAFFINI, M. SUMAN, B. MELEGARI, A. ZAPPETTINI, L. ZANOTTI, U. CASELLATO, M. CARERI AND A. MANGIA (2011). "DEVELOPMENT OF A COMBINED SEM AND ICP-MS APPROACH FOR THE QUALITATIVE AND QUANTITATIVE ANALYSES OF METAL MICROPARTICLES AND SUB-MICROPARTICLES IN FOOD PRODUCTS." ANALYTICAL AND BIOANALYTICAL CHEMISTRY **401**(4): 1401-1409.

BENN, T. B. AND P. WESTERHOFF (2008). "NANOPARTICLE SILVER RELEASED INTO WATER FROM COMMERCIALLY AVAILABLE SOCK FABRICS." ENVIRON. SCI. TECHNOL. **ASAP ONLINE ARTICLE**.

BOOTZ, A., V. VOGEL, D. SCHUBERT AND J. KREUTER (2004). "COMPARISON OF SCANNING ELECTRON MICROSCOPY, DYNAMIC LIGHT SCATTERING AND ANALYTICAL ULTRACENTRIFUGATION FOR THE SIZING OF POLY(BUTYL CYANOACRYLATE) NANOPARTICLES." EUROPEAN JOURNAL OF PHARMACEUTICS AND BIOPHARMACEUTICS **57**(2): 369-375.

BOROWIEC, J. A., A. W. BOORN, J. H. DILLARD, M. S. CRESSER, R. F. BROWNER AND M. J. MATTESON (1980). "INTERFERENCE EFFECTS FROM AEROSOL IONIC REDISTRIBUTION IN ANALYTICAL ATOMIC SPECTROMETRY." ANALYTICAL CHEMISTRY **52**(7): 1054-1059.

BOROVINSKAYA, O., B. HATTENDORF, M. TANNER, S. GSCHWIND AND D. GUNTHER (2013). "A PROTOTYPE OF A NEW INDUCTIVELY COUPLED PLASMA TIME-OF-FLIGHT MASS SPECTROMETER PROVIDING TEMPORALLY RESOLVED, MULTI-ELEMENT DETECTION OF SHORT SIGNALS GENERATED BY SINGLE PARTICLES AND DROPLETS." JOURNAL OF ANALYTICAL ATOMIC SPECTROMETRY **28**(2): 226-233.

BOUWMEESTER, H., I. LYNCH, H. J. P. MARVIN, K. A. DAWSON, M. BERGES, D. BRAGUER, H. J. BYRNE, A. CASEY, G. CHAMBERS, M. J. D. CLIFT, G. ELIA, T. F. FERNANDES, L. B. FJELLSBO, P. HATTO, L.

JUILLERAT, C. KLEIN, W. G. KREYLING, C. NICKEL, M. RIEDIKER AND V. STONE (2011). "MINIMAL ANALYTICAL CHARACTERIZATION OF ENGINEERED NANOMATERIALS NEEDED FOR HAZARD ASSESSMENT IN BIOLOGICAL MATRICES." NANOTOXICOLOGY **5**(1): 1-11.

BUZEA, C., PACHECO, II AND K. ROBBIE (2007). "NANOMATERIALS AND NANOPARTICLES: SOURCES AND TOXICITY." BIOINTERPHASES **2**(4): MR17-MR71.

CHITHRANI, B. D. AND W. C. W. CHAN (2007). "ELUCIDATING THE MECHANISM OF CELLULAR UPTAKE AND REMOVAL OF PROTEIN-COATED GOLD NANOPARTICLES OF DIFFERENT SIZES AND SHAPES." NANO LETTERS **7**(6): 1542-1550.

CHITHRANI, B. D., A. A. GHAZANI AND W. C. W. CHAN (2006). "DETERMINING THE SIZE AND SHAPE DEPENDENCE OF GOLD NANOPARTICLE UPTAKE INTO MAMMALIAN CELLS." NANO LETTERS **6**(4): 662-668.

CHOI, O., K. K. DENG, N. J. KIM, L. ROSS, R. Y. SURAMPALLI AND Z. Q. HU (2008). "THE INHIBITORY EFFECTS OF SILVER NANOPARTICLES, SILVER IONS, AND SILVER CHLORIDE COLLOIDS ON MICROBIAL GROWTH." WATER RESEARCH **42**(12): 3066-3074.

CICHOCKI, B. AND B. U. FELDERHOF (1988). "SHORT-TIME DIFFUSION-COEFFICIENTS AND HIGH-FREQUENCY VISCOSITY OF DILUTE SUSPENSIONS OF SPHERICAL BROWNIAN PARTICLES." JOURNAL OF CHEMICAL PHYSICS **89**(2): 1049-1054.

COLE, K. D., L. F. PEASE, D. H. TSAI, T. SINGH, S. LUTE, K. A. BRORSON AND L. L. WANG (2009). "PARTICLE CONCENTRATION MEASUREMENT OF VIRUS SAMPLES USING ELECTROSPRAY DIFFERENTIAL MOBILITY ANALYSIS AND QUANTITATIVE AMINO ACID ANALYSIS." JOURNAL OF CHROMATOGRAPHY A **1216**(30): 5715-5722.

DEGUELDRE, C. (2003). "COLLOID ANALYSIS BY SINGLE PARTICLE INDUCTIVELY COUPLED PLASMA-MASS." COLLOIDS AND SURFACES A-PHYSICOCHEMICAL AND ENGINEERING ASPECTS **217**(1-3): 137-142.

DEGUELDRE, C. (2004). "THORIUM COLLOID ANALYSIS BY SINGLE PARTICLE INDUCTIVELY COUPLED." TALANTA **62**(5): 1051-1054.

DEGUELDRE, C. (2004). "ZIRCONIA COLLOID ANALYSIS BY SINGLE PARTICLE INDUCTIVELY COUPLED." ANALYTICA CHIMICA ACTA **518**(1-2): 137-142.

DEGUELDRE, C. (2006). "GOLD COLLOID ANALYSIS BY INDUCTIVELY COUPLED PLASMA-MASS SPECTROMETRY." ANALYTICA CHIMICA ACTA **555**(2): 263-268.

DEGUELDRE, C. (2006). "URANIUM COLLOID ANALYSIS BY SINGLE PARTICLE INDUCTIVELY COUPLED." TALANTA **68**(3): 623-628.

DEGUELDRE, C. AND P. Y. FAVARGER (2003). "COLLOID ANALYSIS BY SINGLE PARTICLE INDUCTIVELY COUPLED PLASMA-MASS SPECTROSCOPY: A FEASIBILITY STUDY." COLLOIDS AND SURFACES A-PHYSICOCHEMICAL AND ENGINEERING ASPECTS **217**(1-3): 137-142.

DUBASCOUX, S., I. LE HECHO, M. HASSELLOV, F. VON DER KAMMER, M. P. GAUTIER AND G. LESPES (2010). "FIELD-FLOW FRACTIONATION AND INDUCTIVELY COUPLED PLASMA MASS SPECTROMETER COUPLING: HISTORY, DEVELOPMENT AND APPLICATIONS." JOURNAL OF ANALYTICAL ATOMIC SPECTROMETRY **25**(5): 613-623.

DUDKIEWICZ, A., K. TIEDE, K. LOESCHNER, L. H. S. JENSEN, E. JENSEN, R. WIERZBICKI, A. B. A. BOXALL AND K. MOLHAVE (2011). "CHARACTERIZATION OF NANOMATERIALS IN FOOD BY ELECTRON MICROSCOPY." TRAC-TRENDS IN ANALYTICAL CHEMISTRY **30**(1): 28-43.

DZIEWATKOSKI, M. P., L. B. DANIELS AND J. W. OLESIK (1996). "TIME RESOLVED INDUCTIVELY COUPLED PLASMA MASS SPECTROMETRY MEASUREMENTS WITH INDIVIDUAL, MONODISPERSE DROP SAMPLE INTRODUCTION." ANALYTICAL CHEMISTRY **68**(7): 1101-1109.

EHARA, K. AND H. SAKURAI (2010). "METROLOGY OF AIRBORNE AND LIQUID-BORNE NANOPARTICLES: CURRENT STATUS AND FUTURE NEEDS." METROLOGIA **47**(2): S83-S90.

FABREGA, J., S. N. LUOMA, C. R. TYLER, T. S. GALLOWAY AND J. R. LEAD (2011). "SILVER NANOPARTICLES: BEHAVIOUR AND EFFECTS IN THE AQUATIC ENVIRONMENT." ENVIRONMENT INTERNATIONAL **37**(2): 517-531.

FARKAS, J., H. PETER, P. CHRISTIAN, J. A. G. URREA, M. HASSELLOV, J. TUORINIEMI, S. GUSTAFSSON, E. OLSSON, K. HYLLAND AND K. V. THOMAS (2011). "CHARACTERIZATION OF THE EFFLUENT FROM A NANOSILVER PRODUCING WASHING MACHINE." ENVIRONMENT INTERNATIONAL **37**(6): 1057-1062.

FILELLA, M. (2007). COLLOIDAL PROPERTIES OF SUBMICRON PARTICLES IN NATURAL WATERS. ENVIRONMENTAL COLLOIDS AND PARTICLES: BEHAVIOUR, STRUCTURE AND CHARACTERIZATION. K. J. WILKINSON AND J. R. LEAD. CHICHESTER, JOHN WILEY AND SONS. **10:** 17-93.

GOLDSTEIN, J., D. NEWBURY, D. JOY, C. LYMAN, P. ECHLIN, E. LIFSHIN, L. SAWYER AND J. MICHAEL (2003). SCANNING ELECTRON MICROSCOPY AND X-RAY MICROANALYSIS. NEW YORK, KLUWER ACADEMIC.

GOTTSCHALK. F, S. T., NOWACK B, (2013). "ENVIRONMENTAL CONCENTRATIONS OF ENGINEERED NANOMATERIALS: REVIEW OF MODELING AND ANALYTICAL STUDIES." ENVITRONMENTAL POLLUTION **181**: 287-300.

GSCHWIND, S., L. FLAMIGNI, J. JOACHIM KOCH, O. OLGA BOROVINSKAYA, S. SEBASTIAN GROH, K. KAY NIEMAX AND D. GUNTHER (2011). "CAPABILITIES OF INDUCTIVELY COUPLED PLASMA MASS SPECTROMETRY FOR THE DETECTION OF NANOPARTICLES CARRIED BY MONODISPERSE MICRODROPLETS." JOURNAL OF ANALYTICAL ATOMIC SPECTROMETRY **26**: 1166-1174.

GSCHWIND, S., H. HAGENDORFER, D. A. FRICK AND D. GUNTHER (2013). "MASS QUANTIFICATION OF NANOPARTICLES BY SINGLE DROPLET CALIBRATION USING INDUCTIVELY COUPLED PLASMA MASS SPECTROMETRY." ANALYTICAL CHEMISTRY **85**(12): 5875-5883.

HANDY, R. D., F. VON DER KAMMER, J. R. LEAD, M. HASSELLÖV, R. OWEN AND M. CRANE (2008). "THE ECOTOXICOLOGY AND CHEMISTRY OF MANUFACTURED NANOPARTICLES." ECOTOXICOLOGY **17**: 287–314.

HANSEN, S. F., A. MAYNARD, A. BAUN AND J. A. TICKNER (2008). "LATE LESSONS FROM EARLY WARNINGS FOR NANOTECHNOLOGY." NATURE NANOTECHNOLOGY **3**(8): 444-447.

HARTMANN, G., C. HUTTERER AND M. SCHUSTER (2013). "ULTRA-TRACE DETERMINATION OF SILVER NANOPARTICLES IN WATER SAMPLES USING

CLOUD POINT EXTRACTION AND ETAAS." JOURNAL OF ANALYTICAL ATOMIC SPECTROMETRY **28**(4): 567-572.

HARTMANN, G. AND M. SCHUSTER (2013). "SPECIES SELECTIVE PRECONCENTRATION AND QUANTIFICATION OF GOLD NANOPARTICLES USING CLOUD POINT EXTRACTION AND ELECTROTHERMAL ATOMIC ABSORPTION SPECTROMETRY." ANALYTICA CHIMICA ACTA **761**: 27-33.

HASSELLOV, M., J. W. READMAN, J. F. RANVILLE AND K. TIEDE (2008). "NANOPARTICLE ANALYSIS AND CHARACTERIZATION METHODOLOGIES IN ENVIRONMENTAL RISK ASSESSMENT OF ENGINEERED NANOPARTICLES." ECOTOXICOLOGY **17**(5): 344-361.

HOCHELLA, M. F., S. K. LOWER, P. A. MAURICE, R. L. PENN, N. SAHAI, D. L. SPARKS AND B. S. TWINING (2008). "NANOMINERALS, MINERAL NANOPARTICLES, AND EARTH SYSTEMS." SCIENCE **319**: 631-635.

HOCHELLA, M. F., J. N. MOORE, U. GOLLA AND A. PUTNIS (1999). "A TEM STUDY OF SAMPLES FROM ACID MINE DRAINAGE SYSTEMS: METAL-MINERAL ASSOCIATION WITH IMPLICATIONS FOR TRANSPORT." GEOCHIMICA ET COSMOCHIMICA ACTA **63**(19-20): 3395-3406.

HOLMBERG, J. P., Z. ABBAS, E. AHLBERG, M. HASSELLOV AND J. BERGENHOLTZ (2011). "NONLINEAR CONCENTRATION DEPENDENCE OF THE COLLECTIVE DIFFUSION COEFFICIENT OF TIO(2) NANOPARTICLE DISPERSIONS." JOURNAL OF PHYSICAL CHEMISTRY C **115**(28): 13609-13616.

HORNER, J. A., G. C. Y. CHAN, S. A. LEHN AND G. M. HIEFTJE (2008). "COMPUTERIZED SIMULATION OF SOLUTE-PARTICLE VAPORIZATION IN AN INDUCTIVELY COUPLED PLASMA." SPECTROCHIMICA ACTA PART B-ATOMIC SPECTROSCOPY **63**(2): 217-233.

HORNER, J. A., S. A. LEHN AND G. M. HIEFTJE (2002). "COMPUTERIZED SIMULATION OF AEROSOL-DROPLET DESOLVATION IN AN INDUCTIVELY COUPLED PLASMA." SPECTROCHIMICA ACTA PART B-ATOMIC SPECTROSCOPY **57**(6): 1025-1042.

HOUK, R. S., R. K. WINGE AND X. S. CHEN (1997). "HIGH SPEED PHOTOGRAPHIC STUDY OF WET DROPLETS AND SOLID PARTICLES IN THE INDUCTIVELY COUPLED PLASMA." JOURNAL OF ANALYTICAL ATOMIC SPECTROMETRY **12**(10): 1139-1148.

JORABCHI, K., K. KAHEN, C. GRAY AND A. MONTASER (2005). "IN SITU VISUALIZATION AND CHARACTERIZATION OF AEROSOL DROPLETS IN AN INDUCTIVELY COUPLED PLASMA." ANALYTICAL CHEMISTRY **77**(5): 1253-1260.

KAEGI, R., A. ULRICH, B. SINNET, R. VONBANK, A. WICHSER, S. ZULEEG, H. SIMMLER, S. BRUNNER, H. VONMONT, M. BURKHARDT AND M. BOLLER (2008). "SYNTHETIC TIO(2) NANOPARTICLE EMISSION FROM EXTERIOR FACADES INTO THE AQUATIC ENVIRONMENT." ENVIRONMENTAL POLLUTION **156**(2): 233-239.

KAEGI, R., A. VOEGELIN, B. SINNET, S. ZULEEG, H. HAGENDORFER, M. BURKHARDT AND H. SIEGRIST (2011). "BEHAVIOR OF METALLIC SILVER NANOPARTICLES IN A PILOT WASTEWATER TREATMENT PLANT." ENVIRONMENTAL SCIENCE & TECHNOLOGY **45**(9): 3902-3908.

KANAYA, K. AND S. OKAYAMA (1972). "PENETRATION AND ENERGY-LOSS THEORY OF ELECTRONS IN SOLID TARGETS." JOURNAL OF PHYSICS D-APPLIED PHYSICS **5**(1): 43-&.

KAPELLIOS, E. A. AND S. A. PERGANTIS (2012). "SIZE AND ELEMENTAL COMPOSITION OF NANOPARTICLES USING ION MOBILITY SPECTROMETRY WITH INDUCTIVELY COUPLED PLASMA MASS SPECTROMETRY." JOURNAL OF ANALYTICAL ATOMIC SPECTROMETRY **27**(1): 21-24.

KIM, B., C. S. PARK, M. MURAYAMA AND M. F. HOCHELLA (2010). "DISCOVERY AND CHARACTERIZATION OF SILVER SULFIDE NANOPARTICLES IN FINAL SEWAGE SLUDGE PRODUCTS." ENVIRONMENTAL SCIENCE & TECHNOLOGY **44**(19): 7509-7514.

KIM, J. I. AND C. WALTHER (2007). LASER INDUCED BREAKDOWN DETECTION (LIBD). ENVIRONMENTAL COLLOIDS AND PARTICLES: BEHAVIOUR, STRUCTURE AND CHARACTERIZATION. K. J. WILKINSON AND J. R. LEAD. CHICHESTER, JOHN WILEY AND SONS. **10:** 555-612.

KLAINE, S. J., P. J. J. ALVAREZ, G. E. BATLEY, T. F. FERNANDES, R. D. HANDY, D. Y. LYON, S. MAHENDRA, M. J. MCLAUGHLIN AND J. R. LEAD (2008). "NANOMATERIALS IN THE ENVIRONMENT: BEHAVIOR, FATE, BIOAVAILABILITY, AND EFFECTS." ENVIRONMENTAL TOXICOLOGY AND CHEMISTRY **27**(9): 1825-1851.

KORCAKOVA, L., J. HALD AND M. A. J. SOMERS (2001). "QUANTIFICATION OF LAVES PHASE PARTICLE SIZE IN 9CRW STEEL." MATERIALS CHARACTERIZATION **47**(2): 111-117.

KRUG, H. F. AND P. WICK (2011). "NANOTOXICOLOGY: AN INTERDISCIPLINARY CHALLENGE." ANGEWANDTE CHEMIE INTERNATIONAL EDITION **50**(6): 1260-1278.

LABORDA, F., J. JIMENEZ-LAMANA, E. BOLEA AND J. R. CASTILLO (2011). "SELECTIVE IDENTIFICATION, CHARACTERIZATION AND DETERMINATION OF DISSOLVED SILVER(I) AND SILVER NANOPARTICLES BASED ON SINGLE PARTICLE DETECTION BY INDUCTIVELY COUPLED PLASMA MASS SPECTROMETRY." J. ANAL. AT. SPECTROM. **26**: 1362-1671.

LABORDA, F., J. JIMENEZ-LAMANA, E. BOLEA AND J. R. CASTILLO (2011). "SELECTIVE IDENTIFICATION, CHARACTERIZATION AND DETERMINATION OF DISSOLVED SILVER(I) AND SILVER NANOPARTICLES BASED ON SINGLE PARTICLE DETECTION BY INDUCTIVELY COUPLED PLASMA MASS SPECTROMETRY." JOURNAL OF ANALYTICAL ATOMIC SPECTROMETRY **26**(7): 1362-1371.

LABORDA, F., J. JIMENEZ-LAMANA, E. BOLEA AND J. R. CASTILLO (2013). "CRITICAL CONSIDERATIONS FOR THE DETERMINATION OF NANOPARTICLE NUMBER CONCENTRATIONS, SIZE AND NUMBER SIZE DISTRIBUTIONS BY SINGLE PARTICLE ICP-MS." JOURNAL OF ANALYTICAL ATOMIC SPECTROMETRY **28**(8): 1220-1232.

LEE, J., W. J. SHEN, K. PAYER, T. P. BURG AND S. R. MANALIS (2010). "TOWARD ATTOGRAM MASS MEASUREMENTS IN SOLUTION WITH SUSPENDED NANOCHANNEL RESONATORS." NANO LETTERS **10**(7): 2537-2542.

MAJEDI, S. M., B. C. KELLY AND H. K. LEE (2013). "EFFICIENT HYDROPHOBIZATION AND SOLVENT MICROEXTRACTION FOR DETERMINATION OF TRACE NANO-SIZED SILVER AND TITANIUM DIOXIDE IN NATURAL WATERS." ANALYTICA CHIMICA ACTA **789**: 47-57.

MALLOY, A. AND B. CARR (2006). "NANOPARTICLE TRACKING ANALYSIS - THE HALO SYSTEM." PARTICLE & PARTICLE SYSTEMS CHARACTERIZATION **23**(2): 197-204.

MASLIYAH, J. H., G. NEALE, K. MALYSA AND T. G. M. VANDEVEN (1987). "CREEPING FLOW OVER A COMPOSITE SPHERE - SOLID CORE WITH POROUS SHELL." CHEMICAL ENGINEERING SCIENCE **42**(2): 245-253.

MAVROCORDATOS, D., D. PERRET AND G. G. LEPPARD (2007). STRATEGIES AND ADVANCES IN THE CHARACTERIZATION OF ENVIRONMENTAL COLLOIDS BY ELECTRON MICROSCOPY. ENVIRONMENTAL COLLOIDS AND PARTICLES: BEHAVIOUR, STRUCTURE AND CHARACTERIZATION. K. J. WILKINSON AND J. R. LEAD. CHICHESTER, JOHN WILEY AND SONS. **10:** 345-404.

MITRANO, D. M., E. K. LESHER, A. BEDNAR, J. MONSERUD, C. P. HIGGINS AND J. F. RANVILLE (2012). "DETECTING NANOPARTICULATE SILVER USING SINGLE-PARTICLE INDUCTIVELY COUPLED PLASMA-MASS SPECTROMETRY." ENVIRONMENTAL TOXICOLOGY AND CHEMISTRY **31**(1): 115-121.

NEL, A., T. XIA, L. MADLER AND N. LI (2006). "TOXIC POTENTIAL OF MATERIALS AT THE NANOLEVEL." SCIENCE **311**(5761): 622-627.

NOMIZU, T., H. HAYASHI, N. HOSHINO, T. TANAKA, H. KAWAGUCHI, K. KITAGAWA AND S. KANECO (2002). "DETERMINATION OF ZINC IN INDIVIDUAL AIRBORNE PARTICLES BY INDUCTIVELY COUPLED PLASMA MASS SPECTROMETRY WITH DIGITAL SIGNAL PROCESSING." JOURNAL OF ANALYTICAL ATOMIC SPECTROMETRY **17**(6): 592-595.

NOMIZU, T. AND A. MIZUIKE (1986). "ELECTRON-MICROSCOPY OF SUBMICRON PARTICLES IN NATURAL-WATERS - SPECIMEN PREPARATION BY CENTRIFUGATION." MIKROCHIMICA ACTA **1**(1-2): 65-72.

OBERDORSTER, G., V. STONE AND K. DONALDSON (2007). "TOXICOLOGY OF NANOPARTICLES: A HISTORICAL PERSPECTIVE." NANOTOXICOLOGY **1**(1): 2-25.

OLESIK, J. W. AND P. J. GRAY (2012). "CONSIDERATIONS FOR MEASUREMENT OF INDIVIDUAL NANOPARTICLES OR MICROPARTICLES BY ICP-MS: DETERMINATION OF THE NUMBER OF PARTICLES AND THE ANALYTE MASS IN EACH PARTICLE." JOURNAL OF ANALYTICAL ATOMIC SPECTROMETRY **27**(7): 1143-1155.

OLESIK, J. W., J. A. KINZER AND G. J. MCGOWAN (1997). "OBSERVATION OF ATOM AND ION CLOUDS PRODUCED FROM SINGLE DROPLETS OF SAMPLE IN INDUCTIVELY COUPLED PLASMAS BY OPTICAL EMISSION AND LASER-INDUCED FLUORESCENCE IMAGING." APPLIED SPECTROSCOPY **51**(5): 607-616.

PACE, H. E., N. J. ROGERS, C. JAROLIMEK, V. A. COLEMAN, C. P. HIGGINS AND J. F. RANVILLE (2011). "DETERMINING TRANSPORT EFFICIENCY FOR THE PURPOSE OF COUNTING AND SIZING NANOPARTICLES VIA SINGLE PARTICLE INDUCTIVELY COUPLED PLASMA MASS SPECTROMETRY." ANALYTICAL CHEMISTRY **83**(24): 9361-9369.

PATERSON, G., A. MACKEN AND K. V. THOMAS (2011). "THE NEED FOR STANDARDIZED METHODS AND ENVIRONMENTAL MONITORING PROGRAMS FOR ANTHROPOGENIC NANOPARTICLES." ANALYTICAL METHODS **3**(7): 1461-1467.

PERGANTIS, S. A., T. L. JONES-LEPP AND E. M. HEITHMAR (2012). "HYDRODYNAMIC CHROMATOGRAPHY ONLINE WITH SINGLE PARTICLE-INDUCTIVELY COUPLED PLASMA MASS SPECTROMETRY FOR

ULTRATRACE DETECTION OF METAL-CONTAINING NANOPARTICLES." ANALYTICAL CHEMISTRY **84**(15): 6454-6462.

PICCINNO, F., F. GOTTSCHALK, S. SEEGER AND B. NOWACK (2012). "INDUSTRIAL PRODUCTION QUANTITIES AND USES OF TEN ENGINEERED NANOMATERIALS IN EUROPE AND THE WORLD." JOURNAL OF NANOPARTICLE RESEARCH **14**(9).

PLATHE, K. L., F. VON DER KAMMER, M. HASSELLOV, J. N. MOORE, M. MURAYAMA, T. HOFMANN AND M. F. HOCHELLA (2013). "THE ROLE OF NANOMINERALS AND MINERAL NANOPARTICLES IN THE TRANSPORT OF TOXIC TRACE METALS: FIELD-FLOW FRACTIONATION AND ANALYTICAL TEM ANALYSES AFTER NANOPARTICLE ISOLATION AND DENSITY SEPARATION." GEOCHIMICA ET COSMOCHIMICA ACTA **102**: 213-225.

PRAETORIUS, A., R. ARVIDSSON, S. MOLANDER AND M. SCHERINGER (2013). "FACING COMPLEXITY THROUGH INFORMED SIMPLIFICATIONS: A RESEARCH AGENDA FOR AQUATIC EXPOSURE ASSESSMENT OF NANOPARTICLES." ENVIRONMENTAL SCIENCE-PROCESSES & IMPACTS **15**(1): 161-168.

RAU, E. I. AND L. REIMER (2001). "FUNDAMENTAL PROBLEMS OF IMAGING SUBSURFACE STRUCTURES IN THE BACKSCATTERED ELECTRON MODE IN SCANNING ELECTRON MICROSCOPY." SCANNING **23**(4): 235-240.

ROBERTS, G. S., S. YU, Q. L. ZENG, L. C. L. CHAN, W. ANDERSON, A. H. COLBY, M. W. GRINSTAFF, S. REID AND R. VOGEL (2012). "TUNABLE PORES FOR MEASURING CONCENTRATIONS OF SYNTHETIC AND BIOLOGICAL NANOPARTICLE DISPERSIONS." BIOSENSORS & BIOELECTRONICS **31**(1): 17-25.

SAKAGUCHI, T. AND K. EHARA (2011). "PRIMARY STANDARD FOR THE NUMBER CONCENTRATION OF LIQUID-BORNE PARTICLES IN THE 10 TO 20 MU M DIAMETER RANGE." MEASUREMENT SCIENCE & TECHNOLOGY **22**(2).

SCHILLING, G. D., F. J. ANDRADE, J. H. BARNES, R. P. SPERLINE, M. B. DENTON, C. J. BARINAGA, D. W. KOPPENAAL AND G. M. HIEFTJE (2007). "CONTINUOUS SIMULTANEOUS DETECTION IN MASS SPECTROMETRY." ANALYTICAL CHEMISTRY **79**(20): 7662-7668.

SMITH, D. D. AND R. F. BROWNER (1982). "MEASUREMENT OF AEROSOL TRANSPORT EFFICIENCY IN ATOMIC SPECTROMETRY." ANALYTICAL CHEMISTRY **54**(3): 533-537.

STEWART, II AND J. W. OLESIK (1999). "TIME-RESOLVED MEASUREMENTS WITH SINGLE DROPLET INTRODUCTION TO INVESTIGATE SPACE-CHARGE EFFECTS IN PLASMA MASS SPECTROMETRY." JOURNAL OF THE AMERICAN SOCIETY FOR MASS SPECTROMETRY **10**(2): 159-174.

STOLPE, B., M. HASSELLOV, K. ANDERSSON AND D. R. TURNER (2005). "HIGH RESOLUTION ICPMS AS AN ON-LINE DETECTOR FOR FLOW FIELD-FLOW FRACTIONATION; MULTI-ELEMENT DETERMINATION OF COLLOIDAL SIZE DISTRIBUTIONS IN A NATURAL WATER SAMPLE." ANALYTICA CHIMICA ACTA **535**(1-2): 109-121.

STOLPE, B. AND M. HASSELLÖV (2007). "CHANGES IN SIZE DISTRIBUTION OF FRESH WATER NANOSCALE COLLOIDAL MATTER AND ASSOCIATED ELEMENTS ON MIXING WITH SEAWATER." GEOCHIMICA ET COSMOCHIMICA ACTA **71**: 3292–3301.

UTSUNOMIYA, S. AND R. C. EWING (2003). "APPLICATION OF HIGH-ANGLE ANNULAR DARK FIELD SCANNING TRANSMISSION ELECTRON MICROSCOPY, SCANNING TRANSMISSION ELECTRON MICROSCOPY-ENERGY DISPERSIVE X-RAY SPECTROMETRY, AND ENERGY-FILTERED TRANSMISSION ELECTRON MICROSCOPY TO THE CHARACTERIZATION OF NANOPARTICLES IN THE ENVIRONMENT." ENVIRONMENTAL SCIENCE & TECHNOLOGY **37**(4): 786-791.

UTSUNOMIYA, S., K. A. JENSEN, G. J. KEELER AND R. C. EWING (2004). "DIRECT IDENTIFICATION OF TRACE METALS IN FINE AND ULTRAFINE PARTICLES IN THE DETROIT URBAN ATMOSPHERE." ENVIRONMENTAL SCIENCE & TECHNOLOGY **38**(8): 2289-2297.

VANDENBROECK, C., F. LOSTAK AND H. N. W. LEKKERKERKER (1981). "THE EFFECT OF DIRECT INTERACTIONS ON BROWNIAN DIFFUSION." JOURNAL OF CHEMICAL PHYSICS **74**(3): 2006-2010.

VIGIL, G., Z. H. XU, S. STEINBERG AND J. ISRAELACHVILI (1994). "INTERACTIONS OF SILICA SURFACES." JOURNAL OF COLLOID AND INTERFACE SCIENCE **165**(2): 367-385.

WINGE, R. K., J. S. CRAIN AND R. S. HOUK (1991). "HIGH-SPEED PHOTOGRAPHIC STUDY OF PLASMA FLUCTUATIONS AND INTACT AEROSOL-PARTICLES OR DROPLETS IN INDUCTIVELY COUPLED PLASMA MASS-SPECTROMETRY." JOURNAL OF ANALYTICAL ATOMIC SPECTROMETRY **6**(8): 601-&.

VOGEL, R., G. WILLMOTT, D. KOZAK, G. S. ROBERTS, W. ANDERSON, L. GROENEWEGEN, B. GLOSSOP, A. BARNETT, A. TURNER AND M. TRAU (2011). "QUANTITATIVE SIZING OF NANO/MICROPARTICLES WITH A TUNABLE ELASTOMERIC PORE SENSOR." ANALYTICAL CHEMISTRY **83**(9): 3499-3506.